Department of Precision and Microsystems Engineering

Effect of multi-frequency excitation on vibrational energy harvester power output

J.P. Verduijn

Report no : 2024.021
Coach : T.W.A. Blad
Professor : G.J. Verbiest
Specialisation : MSD
Type of report : MSc Thesis
Date : 18 September 2024



Effect of multi-frequency excitation on vibrational energy harvester power output

A case study of how train vibrations affect energy harvester performance

by

J.P. Verduijn

Student Name	Student Number
Jasper Verduijn	4962524

Supervisor:	G.J. Verbiest
Company supervisor:	T.W.A. Blad
Project Duration:	Nov, 2023 - Sept, 2024
Faculty:	Faculty of Mechanical Engineering, Delft

Cover:	Canadarm 2 Robotic Arm Grapples SpaceX Dragon by NASA under CC BY-NC 2.0 (Modified)
Style:	TU Delft Report Style, with modifications by Daan Zwaneveld

TU Delft

Preface

I have been intrigued by technical machines from a young age. I loved playing with technical toys such as K'nex, but what I loved most was building things myself. Water rockets, PVC darts, speakers, treehouses and much more. When I became older I was unsure if I wanted to continue working on technical stuff. Now that I have almost finished my master's, I am confident I have made the right choice. I enjoyed every part of my study in Delft, and the challenges of understanding a variety of topics is what kept me going.
I genuinely hope this thesis contributes to the development of energy harvesters and that it motivates others to set up new research.

J.P. Verduijn
Delft, September 2024

Summary

This thesis focuses on the effects of complex vibrations on piezoelectric energy harvester power output. So far, research has used idealized vibrations to quantify energy harvester power output. This led to commonly used performance metrics, of which the frequency sweep is the most common. Also, this led to models being validated for only these idealized vibrations.

Real-life measurement data from a freight train showed that the vibration power is often spread over a number of dominant frequencies. This fact has the consequence that the acceleration profile shows a distinctive pattern, where the acceleration is constantly rising and falling. This characteristic has not been taken up in the set of idealized vibrations commonly used in research.

Therefore, this thesis investigates the effect of multiple dominant vibrations on power output of a linear cantilever and bistable buckled beam. These test objects are modeled and experimentally tested. From this, conclusions can be drawn about the validity of existing models for these vibrations, and the effect of multiple dominant vibrations on power output.

The results show that existing models can be used to predict output power, but that one needs to be careful with interpreting their output. For a linear harvester, it was shown that an analytic model can predict power output *if* accounting for a shift in eigenfrequency due to unmodelled nonlinearities. Also, it was confirmed that a frequency sweep is a good performance indicator for real-life power output if one has the information to account for the frequency shift. For a bistable harvester, it was found that a numerical model can - on average - accurately predict power output. However, using frequency sweeps as a performance metric for quantifying power output in a multi-frequency environment is not accurate. Results showed that the effective bandwidth, in which a second frequency can contribute to the total power is much smaller than the large bandwidth that is usually indicated in academic literature.

This thesis concludes that the current models for energy harvesting have value, but they can not yet be used to fully describe the dynamics of energy harvesters. Therefore, experimental testing remains important, and current models need to be improved to use them for optimization. Furthermore, it is recommended that multi-frequency frequency sweeps will be used as an additional performance metric to indicate the realistic bandwidth of an energy harvester in multi-frequency environments.

Contents

Preface i

Summary ii

1 Introduction 1
- 1.1 Introduction to energy harvesting . . . 1
- 1.2 Piezoelectric energy harvesting . . . 1
- 1.3 Real world applications . . . 1
- 1.4 Train vibrations . . . 2
- 1.5 Problem statement . . . 2
- 1.6 Thesis outline . . . 2

2 A systematic review of methods to predict energy harvester power output from accelerometer data 3
- 2.1 Introduction . . . 3
- 2.2 Method . . . 4
- 2.3 Background information . . . 4
  - 2.3.1 Theory of linear energy harvesters . . . 4
- 2.4 Theory of nonlinear energy harvesters . . . 5
- 2.5 Vibration types . . . 6
  - 2.5.1 Stationary dominant frequency . . . 6
  - 2.5.2 Nonstationary dominant frequency . . . 6
  - 2.5.3 Noise . . . 7
  - 2.5.4 Shocks . . . 7
- 2.6 Identification of vibration types . . . 8
  - 2.6.1 Fast Fourier Transform & Power Spectral Density . . . 8
  - 2.6.2 Spectrogram . . . 8
- 2.7 Performance prediction . . . 9
  - 2.7.1 Stationary dominant frequency . . . 9
  - 2.7.2 Nonstationary dominant frequency . . . 10
  - 2.7.3 White noise . . . 11
  - 2.7.4 Filtered noise . . . 12
  - 2.7.5 Band-limited noise . . . 12
  - 2.7.6 Shocks . . . 14
- 2.8 Discussion . . . 14
  - 2.8.1 Limitations . . . 14
  - 2.8.2 Future work . . . 15
- 2.9 Conclusion . . . 15

3 Measurement setup & system identification 16
- 3.1 Measurement setup . . . 16
  - 3.1.1 Overview of measurement setup . . . 16
  - 3.1.2 Power measurement . . . 17
  - 3.1.3 Use of the shaker . . . 18
- 3.2 System identification . . . 19
  - 3.2.1 Piezoelectric cantilever . . . 20
  - 3.2.2 Bistable energy harvester . . . 22
- 3.3 Train vibrations . . . 26

4 Effect of multi-frequency vibrations on energy harvester power output and theoretical predictability **29**
4.1 Introduction . . . 30
4.2 Methods . . . 31
4.2.1 Dynamic test setup . . . 31
4.2.2 Energy harvester design . . . 31
4.2.3 Test vibrations . . . 32
4.2.4 Analytical model of piezoelectric cantilever . . . 34
4.2.5 Experimental performance of a piezoelectric cantilever . . . 34
4.2.6 Numerical model of a bistable energy harvester . . . 35
4.2.7 Experimental performance of a bistable energy harvester . . . 35
4.3 Results . . . 35
4.3.1 Linear piezoelectric cantilever . . . 35
4.3.2 Bistable piezoelectric harvester . . . 35
4.4 Discussion . . . 37
4.4.1 Linear design . . . 37
4.4.2 Bistable design . . . 38
4.5 Conclusions . . . 39

5 Reflection, conclusion & recommendations **40**
5.1 Overview of research activities . . . 40
5.1.1 Successes . . . 41
5.1.2 Unsuccesful attempts . . . 41
5.2 Discussion . . . 41
5.3 Conclusions . . . 42
5.4 Recommendations . . . 42
5.4.1 General remarks . . . 42
5.4.2 Futher research directions . . . 43

A Literature review **47**
A.1 Literature review overview . . . 47
A.2 Signal overview . . . 48

B Measurement setup & system identification **49**
B.1 Components and specifications . . . 49
B.2 Labview diagrams . . . 53

C Technical drawings **56**
C.1 PI E-821 Piezoelectric cantilever . . . 56

D Sensitivity analysis piezoelectric cantilever **57**
D.1 Sensitivity analysis . . . 57
D.2 Decreased power output due to mismatch in model and test object . . . 58
D.3 Conclusion . . . 58

E Error analysis & improvements **59**
E.1 Validation of true train vibrations . . . 59
E.2 Unwanted excitation of eigenmode of the shaker . . . 60
E.3 Inconsistencies in bistable design . . . 60
E.4 Unequal acceleration for system identification & testing. . . . 61

1 Introduction

1.1. Introduction to energy harvesting

Energy harvesting is a collective term for different ways of converting energy from an environment to electric potential. Some examples are solar panels, wind turbines, self winding watches or vibration energy harvesters (VEH). The last one is concerned with converting (part of) the kinetic vibration energy of a system to electric potential.

The output power of an energy harvester is dependent on the conversion of energy from the vibrating system into kinetic energy in the energy harvester and the conversion from kinetic energy in the energy harvester into electric potential. The conversion from kinetic energy into a VEH is most efficient when operating in resonance. Matching the eigenfrequency of a mechanical oscillator with the excitation frequency will result in large deflections. A transducer can subsequently convert this mechanical kinetic energy into electric potential. Piezoelectric material is a transducer that is promising because of its high energy density and easy implementation as compared to other transducers such as electromagnetic ones [1].

1.2. Piezoelectric energy harvesting

Piezoelectric materials are materials that generate a charge difference when deformed. This is a result of aligned asymmetric unit cells, where the deformation of the crystal creates a positive and negative side. Since all crystals are aligned within a piezoelectric material, these positive and negative charges add up, and an overall charge is generated.
The charge difference is linearly related to the deformation of the material. However, many piezoelectric materials are brittle. This makes it challenging to find the perfect balance between getting the most performance out of a unit volume of piezoelectric material and not breaking it.

1.3. Real world applications

One of the most promising markets for energy harvesting is powering sensors. Currently, IoT sensors are powered by batteries, which results in the disposal of 78 million batteries each year by 2025 [2]. Since typical condition monitoring sensors only require 3 mW in active state [3], energy harvesting is an interesting solution for environments that require a reliable, long-term, low-power power source.
Freight trains are one of the more specific environments that could benefit from this technique: they contain a high amount of kinetic energy, there is no power source on board (thus there is the need for a power source) and there is a market demand for putting sensors on these vehicles to track their location and monitor the state of the vehicles.
The challenge in this environment lies in designing an energy harvester that harvests energy independent of external environmental factors such as speed, mass of the train, and track state.

1.4. Train vibrations

A characteristic property of train vibrations is that a large amount of the total power is contained in a few frequencies, hence the name 'dominant frequencies'. Therefore, it is logical to design an energy harvester that is most efficient around (one of) these frequencies.
However, a consequence of having a few dominant frequencies is that they will interfere. This interference is known as beating, resulting in a vibration in which the acceleration continuously rises and falls. This creates moments where the amplitude is high and moments where the acceleration is low or even zero.

1.5. Problem statement

Currently, the most found method of quantifying energy harvester performance in design papers is a frequency response; which is generated using a frequency sweep, where the amplitude is constant. This raises the question of how applicable frequency sweeps are for quantifying the power output of an energy harvester if the real-life excitation does not have a constant amplitude. This research tries to answer that question by measuring and modeling the power output of energy harvesters subjected to interfering vibrations and comparing it to the expected power output for a standard frequency sweep. With these results, a conclusion can be made on the contribution of the extra frequency components to the total power output, the validity of linear and nonlinear models under multi-frequency vibrations, and finally, a conclusion on the validity of single-frequency sweeps for determining power output under multi-frequency vibrations.

1.6. Thesis outline

Chapter 2 contains a literature review, in this chapter, an overview is made of existing methods that can be used to predict energy harverster power output for common types of vibrations. The third chapter presents the practical work that was needed to take measurements during the thesis. It can be used as a reference work for the paper, and it is hopefully helpful for future students who will work on vibrational energy harvesters. Chapter 4 is the main chapter of the thesis, which focuses on the problem statement and studies the effect of multiple dominant vibrations for both linear and nonlinear energy harvesters with experimental and theoretical tests. Lastly, chapter 5 contains a reflection, conclusion and recommendation based on the work of the last 10 months.

2

A systematic review of methods to predict energy harvester power output from accelerometer data

Abstract: The application of energy harvesters for powering low-power sensors is a big step in creating large-scale wireless sensor networks. This paper presents a systematic review of published methods that can be used to analyze the vibrations in an environment to calculate the power output of physics-based piezoelectric energy harvester using analytical methods. The paper analyzes stationary dominant vibrations, nonstationary dominant vibrations, white noise, filtered noise, band-limited noise, and shocks. Methods found are applicable to linear, nonlinear monostable and nonlinear bistable energy harvesters. For linear energy harvesters performance can be calculated using direct analytical formulas or by using the linearity principle in the frequency domain. Nonlinear harvesters can be modelled using the method of multiple scales for stationary dominant vibrations, and with the Fokker-Planck equation for noisy vibrations.

Keywords: energy harvesting, vibration, piezoelectric, signal identification, performance prediction

2.1. Introduction

Technological innovation enables the production of smaller chips and sensors, which are electrically even more efficient. When using many sensors, wireless sensor networks (WSN) can be set up. By constantly measuring environment variables (such as temperature or acceleration), these sensors networks can provide insight into the state of the environment. An example is a train, where the sensor data can be used to gain insight about the state of the train and rail track to perform predictive maintenance [4]. Existing WSN are powered by batteries which need occasional replacements. Currently, this finite lifetime holds back the large-scale employment of sustainable WSN [5]. Also, it would lead to a substantial increase in battery waste: it was calculated that 78 million batteries will be dumped every day by 2025 from powering IoT devices [6]. A solution to this problem would be a self-sustainable device that is powered from its environment, a concept known as energy harvesting. Many industrial environments in which WSN could be employed are subjected to vibrations; therefore electromagnetic, electrostatic, or piezoelectric energy conversion are three possible solutions to convert kinetic energy into electric potential. Since piezoelectric transducers have a high energy density and simple implementation, they are the focus of this research [7]. Traditional energy harvesters are based on the principle of resonance [8]. However, resonance requires stationary harmonic vibrations which often do not exist in real-life. Rantz showed that 72% of the total vibration power in vehicles is nonstationary or can classified as noise [9]. The shift in frequency over time causes a mismatch between the natural frequency and the excitation frequency. That, together with the narrow bandwidth of linear energy harvesters, lowers the amplitude under real-life vibrations and therefore output power. Therefore, current research is moving towards nonlinear energy harvesters,

with the motivation that nonlinearity could lead to a higher bandwidth [8]. This higher bandwidth could be beneficial in harvesting nonstationary signals since it can extract energy over a larger range of frequencies, possibly leading to a higher power output in real-life environments. Wang showed this experimentally; by inducing nonlinearity to a linear cantilever with stoppers, he extended the bandwidth from 13 Hz to 24 Hz [10].

However, this increased bandwidth only says something about the performance in simulations or experimental settings, therefore it is not clear how big its effect is on the power output under real-world vibrations. Therefore, the goal of this paper is to create a systematic overview on how to analyze measurement data from an accelerometer to identify vibration characteristics and use this knowledge to predict the electrical power output of a physics-based model of an energy harvester. The paper provides insight into the relation between types of vibration that occur in real-life and harvestable energy. This understanding could in a later stage potentially be employed to optimize energy harvester designs for specific environments. This is done by splitting the literature review up into the following three parts: Vibration types Defining the different types of vibrations. An overview is made of the different types of vibrations that are generally discussed in literature about energy harvesting. These types do not directly cover all-types of vibration that can occur, however, they can be seen as 'building blocks'. Where a combination of the different types of vibration can accurately describe real-life vibrations. Identification of vibration types Discussing visualization methods that can be used to distinguish the different type of vibrations in an accelerometer measurement. Performance prediction Giving an overview of analytic methods that can be used to predict the power output of a physics-based energy harvester. To make this paper applicable to various energy harvester designs, this paper investigates linear, nonlinear monostable and nonlinear bistable energy harvesters.

2.2. Method

Per section different keywords are used to search for information, which can be found in section A.1. Literature databases used are Scopus and Google Scholar. Scopus was used because of its extensive filtering options and Google Scholar was useful when performing broader searches to explore topics. Also, referenced papers were used to trace back derivations and assumptions. The quality of papers was checked by the clarity of the results, checking how many citations the author has and by checking if the author is specialized in the field that corresponds to the paper.

2.3. Background information

2.3.1. Theory of linear energy harvesters

Linear energy harvesters are commonly modelled as a single degree of freedom mass-spring-damper systems (Figure 2.1), its dynamics can be described by Eq. 1 under the assumption that the base is excited by $y(t) = Ysin(\omega t)$.

$$m\ddot{x} + c\dot{x} + kx = -m\omega^2 Y \sin(\omega t) \tag{2.1}$$

Here, m is the oscillating mass, c is the damping, k is the spring stiffness, x is the displacement of the mass, Y is the maximum amplitude of the displacement, ω is the driving frequency of the base and t is the time.

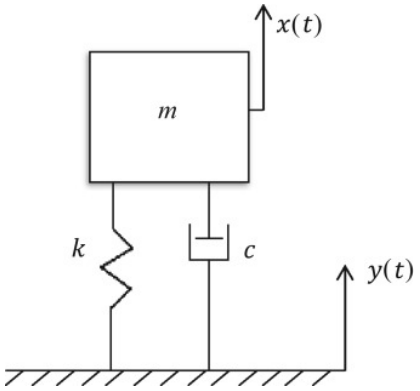


Figure 2.1: Physics model of linear energy harvester

The coupling with the electrical domain in this model is represented as a part of c (velocity-dependent damping) which is a reasonable assumption [11]. Following the derivations from Stephen, the average power flow into the whole system in dimensionless form can be expressed as [12]:

$$P_{\text{avg}} = \frac{m\zeta_t Y^2 \left(\frac{\omega}{\omega_n}\right)^3 \omega^3}{\left(1 - \left(\frac{\omega}{\omega_n}\right)^2\right)^2 + \left(2\zeta_t \frac{\omega}{\omega_n}\right)^2} \tag{2.2}$$

Where ζ is the total damping ratio of the system and ω_n is the resonant frequency. Under the assumption that the damping ratio is small ($\zeta < 0.3$), one may assume that the resonant frequency of base excitation is the same as the one from direct mass excitation [12]. The system will then operate optimally at its resonant frequency. In this case ($\omega = \omega_n$), the power transfer becomes:

$P_{(avg,res)} = \omega_n^3 m Y^2/(4\zeta)$. However, in many real-life situations it is near impossible to have the resonant frequency of the system match the excitation frequency. This causes the power transfer into the device to decrease drastically decrease (Figure 2.2). A mismatch of 2% from the resonance frequency already decreases the performance of the device by 50% for $\omega_t = 0.02$. Since vibrations in nature never consist of a constant frequency, researchers started exploring nonlinear energy harvesters which are more robust.

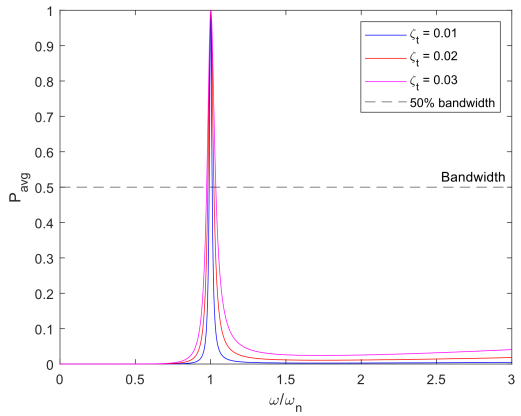


Figure 2.2: Plot of Eq. 2 for different total damping ratios to visualize how to power output scales when the excitation frequency mismatches the resonance frequency of the system.

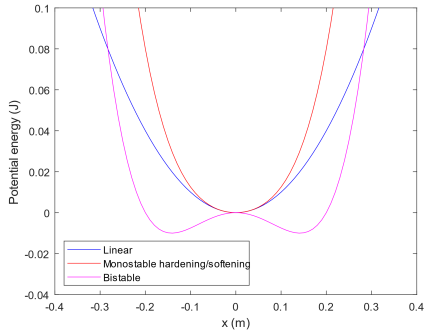


Figure 2.3: Visualization of Eq. 4 for different parameters (see Table 2.1) that categorize the different types of energy harvesters

	r	δ
Linear	$r < 1$	$\delta = 0$
Monostable softening	$r \leq 1$	$\delta < 0$
Monostable hardening	$r \leq 1$	$\delta < 0$
Bistable	$r > 1$	$\delta > 0$

Table 2.1: Parameters that define the groups displayed in this table, which define the different types of dynamics

2.4. Theory of nonlinear energy harvesters

Most papers related to nonlinear energy harvesting discuss intentional introduction of nonlinear stiffness. Thus, the damping and inertia are assumed to be linear. For this case, the dynamics of a nonlinear energy harvester is described by Eq. 3 [13].

$$m\ddot{x} + c\dot{x} + \frac{dU(x)}{dx} = -m\ddot{y} \tag{2.3}$$

Here U(x) represents the restoring force, which is characterized by Eq. 4 [13].

$$U(x) = \frac{1}{2}k_1(1-r)x^2 + \frac{1}{4}k_3x^4 \tag{2.4}$$

Where k_1 is the linear stiffness, k_3 is the nonlinear stiffness and r is a tuning parameter. Defining the nonlinearity strength as $\delta = k_3/k_1$, three nonlinear types of dynamical systems can be recognized by plotting U(x) (Table 1 & Figure 2.3).

Substitution of δ and Eq. 4 in Eq. 3 gives the Duffing equation (Eq. 5) [13]. This type of model is commonly used in the modelling of nonlinear energy harvesters.

$$\ddot{x} + 2\zeta_t\dot{x} + (1-r)x + \zeta_t x^3 = -y \tag{2.5}$$

A motivation for using bistable energy harvesters is so-called snap-through behavior, where the system switches between the two stable states (see interwell motion in Figure 2.5). This snap-through behavior increases the velocity of the mass. Since the output power scales with velocity squared, this means the bistable system has the potential of having a higher power output than intrawell motion [8]. Besides, the snap-trough motion can be triggered independent of the excitation frequency which can improve the bandwidth of the energy harvester and thus improve its overall performance [14].

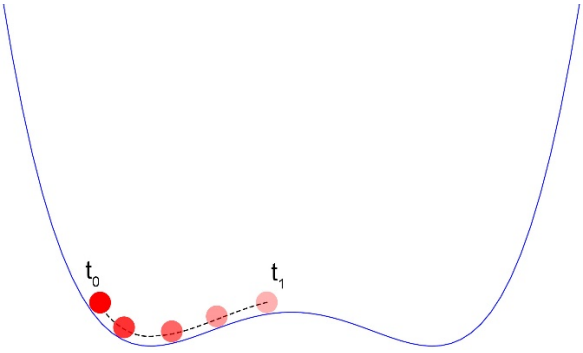


Figure 2.4: Intrawell motion - Travelling around one stable point

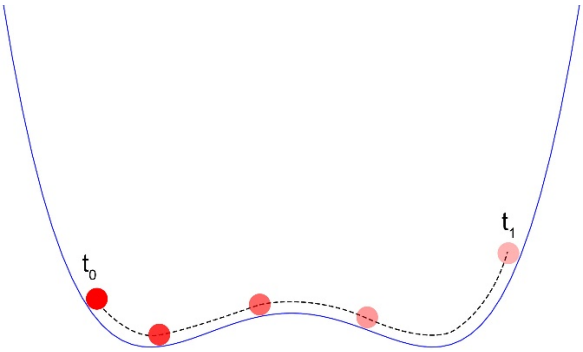


Figure 2.5: Interwell motion – Travelling between two stable states (snap-through motion)

2.5. Vibration types

Existing methods on performance prediction perform analysis per type of vibration. To use these methods, it is therefore first important to make an overview of the types of vibrations characteristics that occur in real-life, to determine which performance prediction method to use for a certain environment. The presented classification is an overview of common types of vibrations found in books about vibration theory and papers related to energy harvesting. A limitation is thus that these are idealized vibrations. Real-life vibrations are more complex since they contain a variety of frequencies, or their frequency spectrum does not directly correspond to one of the idealized types of vibrations. The types of vibrations in this section should be seen as 'building blocks', where combination of multiple building blocks together can closely approximate real-life vibrations.

2.5.1. Stationary dominant frequency

The ideal signal for resonance-based energy harvesters is a harmonic oscillation with a fixed frequency and amplitude. Its displacement and acceleration are described by Eq. 6 and Eq. 7 respectively.

$$y(t) = Ysin(\omega t) \tag{2.6}$$

$$\ddot{y}(t) = -Y\omega^2 sin(\omega t) \tag{2.7}$$

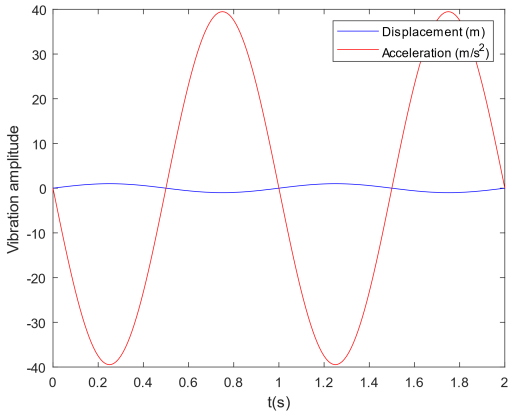


Figure 2.6: Eq. 6 and Eq. 7 for $\omega = 2\pi$

Both are visualized in Figure 2.6.

An example of an environment where this vibration occurs is a motor-powered machine in a factory with a constant load and speed. The vibration is classified as stationary since its properties do not depend on time.

2.5.2. Nonstationary dominant frequency

A more representative vibration of the stationary vibration one with amplitude modulation (AM) (Eq. 8) or amplitude-frequency modulation (AM-FM) (Eq. 9) [15].

$$y(t) = (Y_0 + \sigma(t))cos(\omega t) \tag{2.8}$$

$$y(t) = (Y_0 + \sigma(t)) \cos\left(\int_0^t (\omega t + \epsilon(t))\, dt\right) \tag{2.9}$$

Where $\sigma(t)$ represents the offset from the central amplitude Y_0 by white gaussian noise and $\epsilon(t)$ represents the frequency deviation by white gaussian noise. Examples of environments where this signal could occur are a driveshaft of a machine with varying speed (frequency modulation) or a car driving with a constant speed over a varying road surface (amplitude modulation). This signal is classified as a nonstationary signal since its properties depend on time.

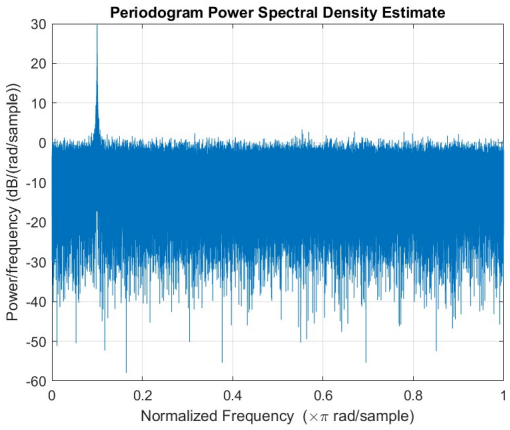


Figure 2.8: Power spectral density of AM/FM modulated signal

2.5.3. Noise

Noise signals do not show a pattern in the time-domain. In the frequency domain however, there is a correlation between the amplitude across different frequencies.

White noise

The simplest type of noise is white noise. Its properties are that the signal consists of uncorrelated values and that it has a flat power spectral density with intensity S_{xx}.

$$S(\omega) = S_{xx} \tag{2.10}$$

White noise is classified as a stationary signal and is seen in 23% of the environments with machines [9]. It occurs in systems with high damping, that causes the energy to spread over a wide range of frequencies.

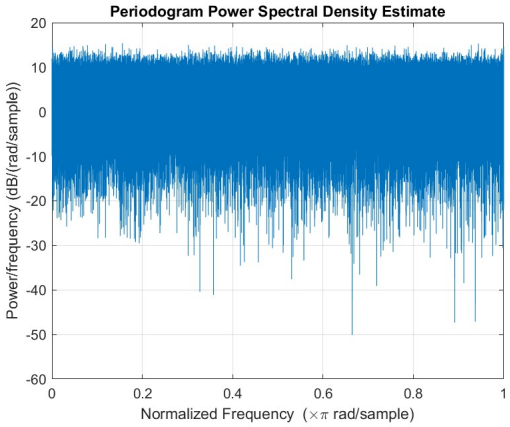


Figure 2.9: Power spectral density of white noise.

Filtered noise

Filtered noise is a variant of white noise, where the power spectral density is not flat, but contains a visual relationship and continuous power. An example could be white noise passed through a low-pass or high-pass filter. In 55% percent of mechanical structures there is filtered noise since mechanical structures act as a filter [9].

$$S(\omega) = filter(\omega) \cdot S_{xx} \tag{2.11}$$

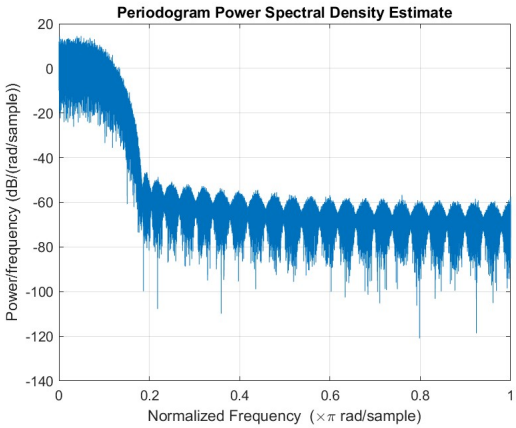


Figure 2.10: Power spectral density of filtered noise.

Band-limited noise

Whereas white and filtered noise contain a continuous finite power spectral density, band-limited noise only contains power across a small bandwidth. This can be seen as white noise passed through a band-pass filter.

$$S(\omega) = bandpassfilter(\omega) \cdot S_{xx} \tag{2.12}$$

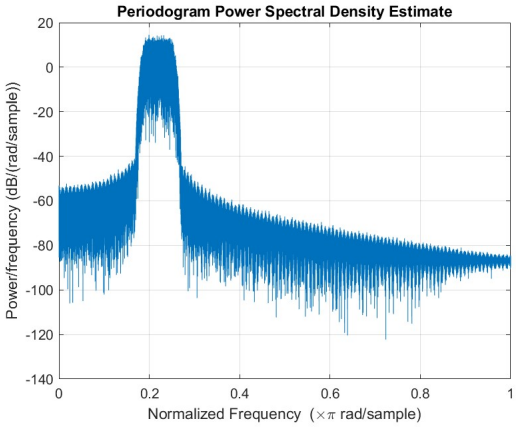


Figure 2.11: Power spectral density of band-limited noise.

2.5.4. Shocks

Shocks are defined as a transmission of kinetic energy which takes place in a relatively short time

compared with the natural frequency of oscillation of the system [16]. This impulse in energy is generally described by half a period of a sine wave, also called a half-sine shock.

$$x(t) = A_{shock} \sin(\omega t) \quad 0 < t < \frac{\pi}{\omega} \tag{2.13}$$

Where A_{shock} is the amplitude of the shock.

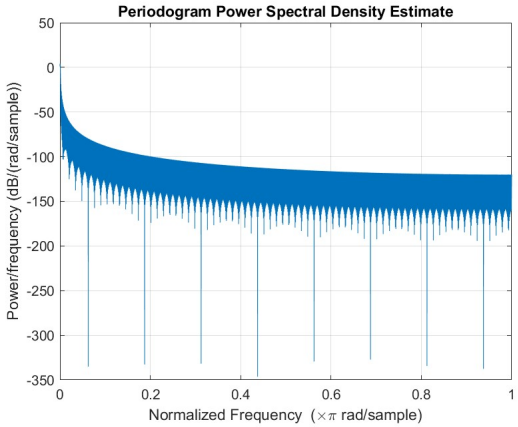


Figure 2.12: Power spectral density of half-sine shock.

The PSD of the shock shows it contains energy across a wide range of frequencies.

2.6. Identification of vibration types

This section of the paper is concerned with listing different methods that can be used to detect and distinguish the different types of signals discussed in Section 4. First it is important to note that the power transfer from an environment into a linear energy harvesting device is dependent on the excitation frequency (Figure 2.2). Therefore, the methods discussed in this section are based on the Fast Fourier Transformation (FFT) to convert the time-domain data to frequency-domain data.

2.6.1. Fast Fourier Transform & Power Spectral Density

The first method to visualize the frequencies in a signal is the Fast Fourier Transform (FFT). When performing an FFT of an acceleration measurement, the FFT visualizes the magnitude of the vibration across the different frequencies up to the Nyquist frequency. The magnitude is displayed per bin. The bin width determines the resolution of the FFT and its width is determined by the sampling frequency divided by the number of samples. Thus, more samples give a higher resolution. To get a more objective picture of the frequencies in a signal it is therefore important to get a proper resolution. However, the FFT will always be related to the length of signal, making it hard to compare two FFTs with different lengths to each other. The PSD is calculated by multiplying each bin by its complex conjugate. This gives $unit^2$, which translates to g^2 if the accelerometer has the unit g. Next, the amplitude is normalized to the to the frequency bin width. This makes the units g^2/Hz. This is an improvement over the FFT, since it creates an objective measure which can be used to compare signals of different lengths. The PSD can be used to detect dominant frequencies and types of noise. Dominant stationary frequencies will show as narrow peaks, whereas dominant nonstationary frequencies will show up as wider peaks. The PSD is also a useful tool for determining possible (types of) noise, the relation of signal strength over the frequencies can be used to determine types of noise. The limitation of the PSD however is that it captures an entire signal in one graph. This makes it impossible to see how signal properties change over time (stationary vs. non-stationary). This problem is solved by using spectrograms.

2.6.2. Spectrogram

Spectrograms are time-dependent PSDs, that is why they are also called Short-Time Fourier Transform; they show a series of PSDs for small time-segments of a signal. The horizontal axis displays time, the vertical axis displays frequency and the z-axis displays signal power. This provides extra insights about the signal and makes it possible to see how frequencies within a signal change over time (AM and/or FM) and detect shocks. Stationary dominant frequencies will show up as horizontal lines parallel to the time-axis, whereas nonstationary dominant frequencies will show up as non-flat connected lines (FM) or flat connected lines with changing signal power (AM). Determining what frequencies are dominant and which are not may become tedious when a signal contains a wide spectrum of frequencies. One technique to make the identification of dominant frequencies easier, is to filter out frequencies below a threshold value relative to the peak power [9], [17]. When applying this technique one needs to consider that this results in a loss of information.

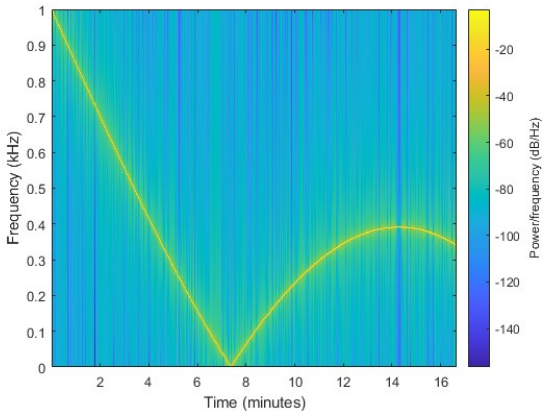


Figure 2.13: Example of spectrogram that shows nonstationary vibration.

Since shocks contain energy across all frequencies [16], shocks show up as vertical lines in the spectrogram. Classification of a sudden increase in energy can be done by looking at the power with respect to a certain threshold, for example the average. Where a shock is detected if the power is larger than the threshold [17]. One limitation of using spectrograms for detecting shocks is its dependency on window size. A large window size decreases the time resolution, which will average out the power from the shock, making it less noticeable.

2.7. Performance prediction

2.7.1. Stationary dominant frequency

Linear

For linear energy harvesters, the total power flow into the device is described by Eq. 2, under the assumption that the base excitation is $y = Ysin(\omega t)$. Here, the total damping ratio ζ_t consists of mechanical damping ζ_m, electrical losses ζ_e loss and damping from the load ζ_e load ($\zeta_t = \zeta_m + \zeta_{(eloss)} + \zeta_{(eload)}$). Therefore, the electrical power that is transferred into the load, which represents the harvested electrical power, is [12]:

$$P_{\text{avg,load}} = \frac{m\zeta_{e,load} y_0^2 \left(\frac{\omega}{\omega_n}\right)^3}{\left(1 - \left(\frac{\omega}{\omega_n}\right)^2\right)^2 + (2\zeta_t \frac{\omega}{\omega_n})^2} \tag{2.14}$$

Note from Eq. 14 that the power scales with $mY^2\omega^3$. When defining the acceleration of the vibration as $\ddot{y} = -Y_0\omega^2 \sin(\omega t)$ (which follows from the assumption of sinusoidal base excitation), one can define A as the amplitude of the vibration, where $A = Y_0\omega^2$. Substituting this result for Y_0 in Eq. 14 yields:

$$P_{\text{avg,load}} = \frac{m\zeta_e \text{load} A^2 \left(\frac{\omega}{\omega_n}\right)^3}{\left(1 - \left(\frac{\omega}{\omega_n}\right)^2\right)^2 + (2\zeta_t \frac{\omega}{\omega_n})^2} \tag{2.15}$$

Using this transformation, one can see the power now scales with mA^2/ω. This is an important result since it confirms that the scale of the PSD from an acceleration measurement (g^2/Hz) is appropriate for identifying and comparing the most powerful frequencies. From the above equation it looks like infinite power can be extracted when decreasing the total damping ratio to (almost) zero. However, this would make the amplitude of the generator infinitely large, which is not possible.

Nonlinear

Monostable The dynamics of nonlinear monostable energy harvesters under stationary harmonic oscillation can be analytically derived using the method of multiple scales [18]. Daqaq performs this derivation and is looking at the steady-state amplitude and phase of the frequency response to study the variation of the steady-state amplitude with the excitation frequency [8]. From the motion the amplitude of the voltage is calculated, to consequently calculate power. The analytical formulation made it possible to draw conclusions on how the backward coupling κ and time constant ratio α affect harvester performance. Where the time constant ratio is the ratio between the time constant of the mechanical oscillator and the electrical circuit, and the backward coupling is defined as $\kappa^2 = \theta/(k_1 C_p)$, where θ is the electromechanical coupling and C_p is the capacitance of the piezoelectric element.

Backward coupling For the backward coupling it was found that increasing κ reduces the amplitude, which is as expected, since it increases the electrical damping. Also, the resonant frequency is increased with an increasement in κ (Figure 2.14). The reduced amplitude does not directly relate to decreased performance, because the reduced amplitude is a consequence of transferring more energy to the electrical domain. It was found that there exists an optimal value of κ for maximum electrical power. Increasing κ beyond this point would further decrease the damping, and with that the velocity and output power (Figure 2.15).

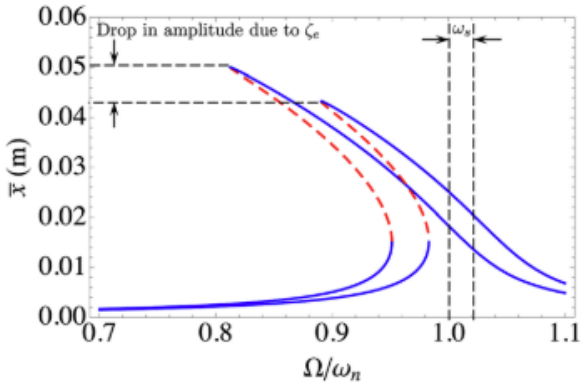


Figure 2.14: Influence of increased damping caused by increased backward coupling κ on frequency response. Retrieved from Daqaq [8]

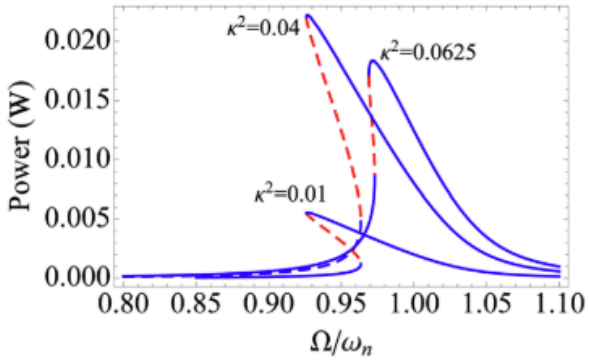


Figure 2.15: Influence of backward coupling κ on output power. Retrieved from Daqaq [8]

Time constant ratio For large and small values of α it was found that the electrical damping is very small; and ζ_e is maximum for $\alpha = 1$. Reducing α widens the bandwidth, but also lowers peak power (Figure 2.16). This concludes that α is an important tuning parameter for nonlinear energy harvester which makes the trade-off between peak power and bandwidth.

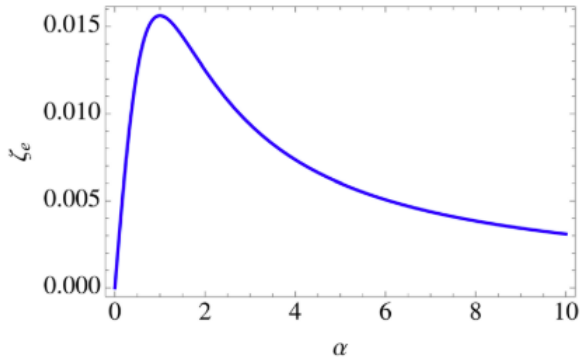


Figure 2.16: Effect of α on the electric damping. Retrieved from Daqaq [8]

Bistable Zhang proposes a method using harmonic balancing for the analysis of output power and the effect of design parameters [19]. The analytical model was validated using a testing setup. For validation a bistable cantilever was used, where bistability was induced via magnets, but the analysis can also be extended to other mechanisms such as clamped-clamped cantilevers with pretension. The analytical analysis was validated both numerically and experimentally and it showed good reliability. From this validated model multiple conclusions could be made: *Excitation level* - Analytical results yield stable and unstable solution branches. In numerical simulations it was found that for low excitation levels the high and low orbit always coexist. For higher levels of excitations, the solution branches span a larger bandwidth and have a higher overall power. *Load resistance and coupling constant* - For the load resistance and coupling constant it was found that there is a frequency dependent optimum. For moderate coupling constants and load resistance the harvested power increases, but for relatively large coupling constants and load resistance the harvested power decreases. This corresponds with the result for backward coupling for monostable energy harvesters.

2.7.2. Nonstationary dominant frequency

Linear

In the case of nonstationary vibrations, the analytical formulas described in 6.1.1 are not applicable anymore. Yoon created a stochastic approach to calculate the harvestable energy of linear energy harvesters under nonstationary vibrations (AM & AM/FM) [20]. The framework consists of three sequentially executed procedures, visualized in Figure 2.17.

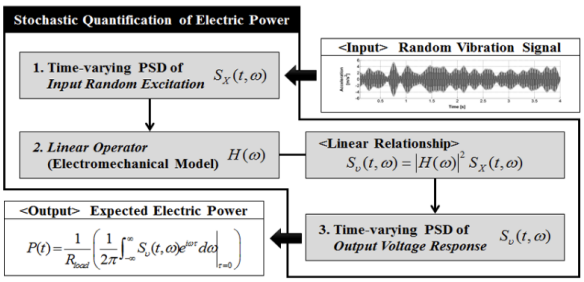


Figure 2.17: Framework for predicting power output. Retrieved from Yoon [20]

Yoon applies an analytical model for a bimorph cantilever-type piezoelectric energy harvester model, established by Erturk & Inman [21]. However, using a different model the approach

of Yoon can be extended to other types of harvesters. It was found that the stochastic approach of Yoon was in good agreement (0.52% error in output power) with the model established by Zhao and Erturk that was validated numerically and experimentally [22]. (The improvement of Yoon's stochastic approach over the model from Zhao and Erturk is that it can model AM/FM signals, whereas the model from Zhao and Erturk was limited to broadband random vibrations.) The differences between the expected electric power from both methods is a result of the bandwidth range. The stochastic approach has a limited bandwidth due to Nyquist, while the numerical approach has an infinite bandwidth. An important sidenote of Yoon's approach is that both AM and AM/FM vibrations where approximated as in Eq. 8 and Eq. 9, thus the offset from the amplitude and central frequency is approximated to be white noise. This approximation might not be valid for all real-life signals. Eguiluz also researched ways to maximize harvested energy under nonstationary vibrations. In the research two identical energy harvesters were compared with different eigenfrequencies. It was found that the highest power was harvested when the eigenfrequency was tuned to the sum of the PSD over time (sum of spectrogram) compared to tuning the eigenfrequency of the harvester to the frequency with peak power in the PSD [23]. This is an interesting result because of its easy and fast implementation. The success of this technique is dependent on the vibration though.

Nonlinear
No methods were found to describe the performance of nonlinear energy harvesters under nonstationary vibrations. This is likely due to the complexity of calculations, as well as the wide type of signals that can be classified as 'nonstationary' which makes it impossible to make general conclusions about it.

2.7.3. White noise

Linear
First, the total power flow under white noise into an energy harvester is defined by Langley as [24]:

$$\frac{\pi S_0 m}{2} = P_M + P_E \tag{2.16}$$

Here S_0 is the single-sided spectral density and P_M and P_E represent the mechanical power and electrical power respectively. This formulation can be used a quick way to quantify the maximum amount of energy that can be harvested. Also, analytical formulas have been set up to calculate power output of linear energy harvesters under white noise using device parameters. The maximum harvested power is defined by $P_{EMaxLin}$ under the conditions stated by Hawes [25]

$$P_{EMaxlin} = \frac{m\theta^2}{(\sqrt{b^2C + \theta^2 m})^2} - \frac{\pi S_0 m}{2} \tag{2.17}$$

Here θ is the electrical coupling coefficient, b is the mechanical damping rate, C is the capacitance of the capacitor.

Nonlinear
Since noise is a stochastic process, nonlinear systems are generally analyzed by computing their probability density functions (PDF), which describes the time evolution of the PDF under random forces. The PDF is generally obtained using the Fokker Plank Equation (for implementation procedure refer to Daqaq [14]). Gammaitoni is one of many researchers that uses this approach. In the analysis he uses a coupled system of equations to describe the mechanical and electric dynamics [26].

$$\dot{x} = -\frac{dU(x)}{dx} - c\dot{x} - K_v V + F(t) \tag{2.18}$$

$$\dot{V} = K_c \dot{x} - \frac{1}{t_p} V \tag{2.19}$$

Here, K_v is the coupling coefficient that relates the oscillation to the voltage, V is the voltage drop, F(t) is a random force (gaussian white noise), K_c is the coupling constant of the piezoelectric sample and τ_p is the time constant. He found that the time constant ratio $\tau_p = RC$, where C is the coupling resistance and R is the load resistance, plays an important role in the performance prediction of nonlinear energy harvesters under noise. From Eq. 19 It can be seen τ_p acts as a highpass filter on V: Therefore, the time constant ratio has te be large enough so that V(t) can follow the displacement of x(t) and the least amount of energy is lost.

Monostable For a large τ_p it was found (both numerically and experimentally) that the output power of the harvester becomes independent of the nonlinearity. In this case linear and nonlinear energy harvesters would have the same performance, which is in line with the findings from Daqaq and Sebald [27][28]. But it was also found that for two identical energy harvesters, but one with nonlinear stiffness, the nonlinear energy harvester had a smaller RMS displacement [29]. This implies a higher energy density; however, it is important to distinguish RMS displacement from maximum displacement when designing an energy harvester.

Bistable Bistable energy harvesters can have an improved performance under white noise vibration, under the condition that the time constant ratio is

very small [30]. For large time constant ratios the same result was found as for monostable energy harvesters: the output power becomes independent of the nonlinearity and the device would have the same performance as a linear energy harvester [31].

2.7.4. Filtered noise

Linear

For monostable nonlinear energy harvesters under filtered noise excitation no analytical performance prediction methods were found.

Nonlinear

Monostable For monostable nonlinear energy harvesters under filtered noise excitation no analytical performance prediction methods were found.

Bistable Daqaq studied the performance of bistable energy harvesters analytically under filtered noise. Calculation of the power output was also done using the Fokker Plank Equation (ref to 6.3.3.), however since the PDF depends on the PDF itself, an iterative procedure was used to calculate an approximate PDF. This approximate PDF was validated using numerical simulation, it was found that the error in the PDF can become as large as 15%, however its shape remains the same, so it is a scaling error. Albeit the error, the results can therefore still be used to get insight into the dynamics of the energy harvester. The research of Daqaq focused on shaping the potential function to optimize power output. Power output was quantified by looking at the mean square velocity. Simulations showed that for different noise intensities different optimal potential shapes exist. A trend was found, where decreasing the separation of the potential wells first increases the mean square velocity up to an optimal point because it increases the frequency of interwell motions, after which the mean square velocity drops since interwell motion does not contribute anymore to a higher average velocity (see Figure 2.18).

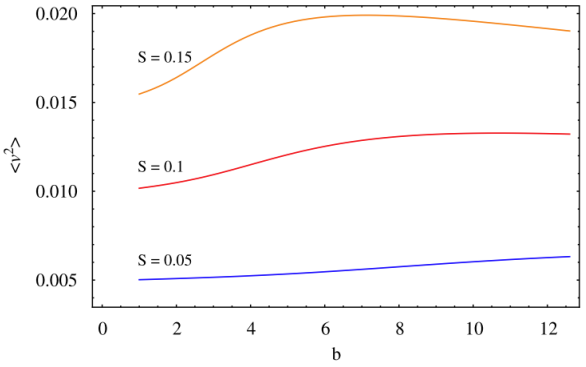


Figure 2.18: Variation of mean square velocity with b, which determines the separation of the potential wells (S is noise intensity, higher b represents smaller separation of potential wells). Retrieved from Daqaq [14].

Simulations at different noise intensities later showed that the potential shape is independent of the noise strength (see Figure 2.19). This is an important result for optimization of the device parameters because it implies that the optimal potential shape is a function of device parameters and the shape of the noise, but not the noise strength.

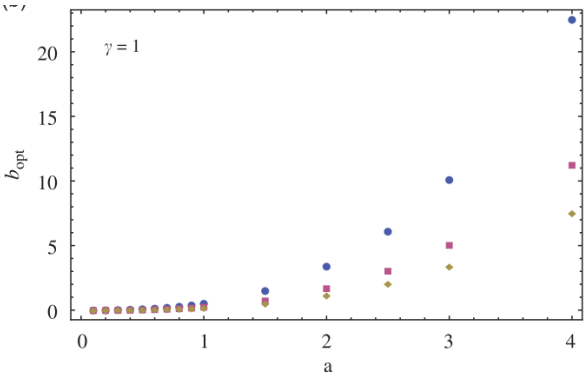


Figure 2.19: Optimal value of b with respect to a for different noise intensities. Blue circles: S = 0.05 Red squares: S = 0.10 Yellow diamonds: S = 0.15. Retrieved from Daqaq [14].

2.7.5. Band-limited noise

Linear

As described in section 4.3.3 band-limited noise can be seen as white noise passed through a bandpass filter. This approach was used by Halvorsen to predict energy harvester power output of a linear energy harvester under band-limited noise. Using a second-order bandpass model and two-part model a formula was made to calculate output power directly without stochastic simulation [32]. Since band-limited noise with a small bandwidth approaches a single frequency, and band-limited noise with a large bandwidth approaches white noise, Halvorsen made a comparison of power output of two optimized energy harvester optimized

for both white noise and a single frequency, under band-limited noise excitation. By varying the bandwidth of the band-limited vibration a crossover point was found where the power output of one of the harvesters outperforms the power output of the other. From Halvorsen's results in Figure 2.20 it can be seen that for a small bandwidth the power of the single-frequency harvesters is almost 20 times as high. For larger bandwidths (approaching white noise), the difference in power output between both harvesters becomes much less. The main conclusion that can be drawn from this is that an energy harvester that is optimized for white noise performs much worse under band-limited noise with a small bandwidth than an energy harvester that is optimized for single frequency, whereas the other way around an energy harvester that is optimized for single frequency excitation has similar performance as an energy harvester that is optimized for white noise under band-limited excitation with a large bandwidth.

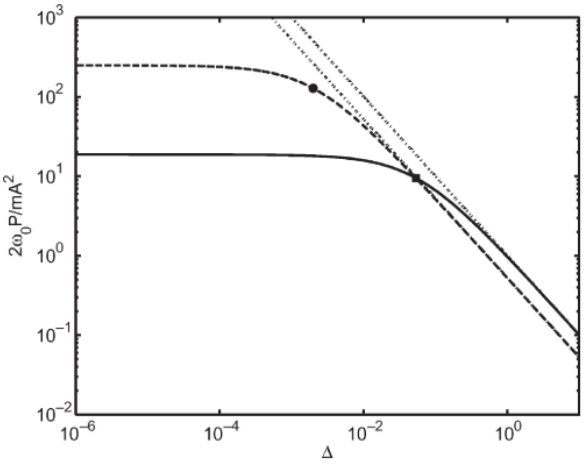


Figure 2.20: Output power (y-axis) for band-limited excitation with varying bandwidth Δ (x-axis). Solid line: energy harvester optimized for white noise. Dashed line: energy harvester optimized for single frequency. Dotted lines: asymptotic wideband performance. Retrieved from Halvorsen [32].

Nonlinear

For nonlinear energy harvesters under band-limited excitation no analytical performance prediction methods were found. This is likely due to the complexity of nonlinear systems and hysteresis. However, Masana studied the performance of nonlinear energy harvesters under band-limited noise experimentally [33]. In the experiment the response of the energy harvester was studied by systematically changing the center frequency f_c of the band-limited noise and the bandwidth Δ of the noise under different excitation levels, both parameters are visualized in Figure 2.21.

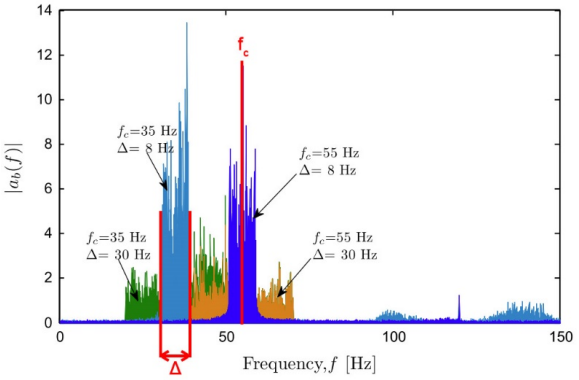


Figure 2.21: Visualization of center frequency f_c and bandwidth Δ. Retrieved from Masana [33].

For the influence of the center frequency, it was found that at small excitation levels both monostable and bistable obtained their peak voltage at their fundamental frequency, leading to the conclusion that the nonlinearity has no effect at small excitations. For higher excitations it was found that the bandwidth of the bistable energy harvester increased by 50% (from 14 Hz to 21 Hz). It was also found that the voltage variance of the bistable energy harvester remained at a high level (33% of peak voltage) for low frequencies, whereas the voltage of the monostable energy harvester quickly decreases far from the fundamental frequency (see Figure 2.22 and Figure 2.23). Masana believes that this is a result of super-harmonics.

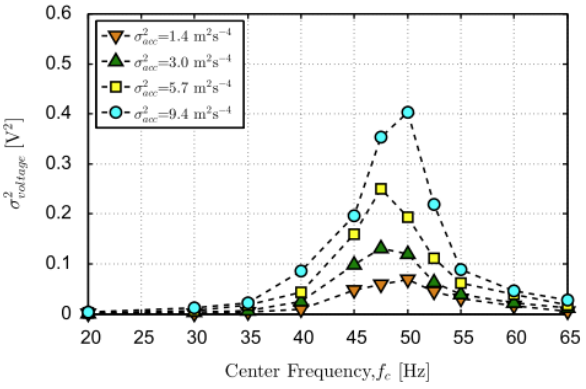


Figure 2.22: Voltage variance at different center frequencies of monostable energy harvester. Retrieved from Masana [33].

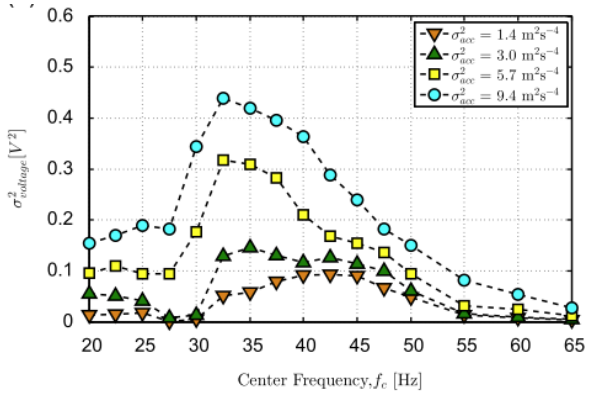


Figure 2.23: Voltage variance at different center frequencies of bistable energy harvester. Retrieved from Masana [33].

2.7.6. Shocks

Linear

Research has shown that frequency matching with a small bandwidth is less important for shock excited energy harvesters [34]. Its dynamic response to a shock can be calculated with the convolution integral of the shock profile and the harvesters' response to a unit shock [34]. Since the bandwidth is less of a concern compared to resonance energy harvesters and high power is related to a high Q-factor, maximum energy is harvested under shock conditions for harvesters with low damping. Schaijk also researched the effect of shock. For square shocks it was found that the optimal duration $t_{shock} = n/2f_n$, with n=1,3,5... [34]. For sine shocks no optimal duration was given. Khaghanifard found that one can use the shock spectral diagram to find optimal shock duration [35]. The amplitude shock diagram provides a good start for finding optimal shock duration, but the power shock diagram provides higher accuracy. Furthermore, a rule of thumb is that the frequency of an optimal half-sine shock is always 10 times smaller than the natural frequency of the system [35].

Nonlinear

Monostable For nonlinear monostable energy harvesters under shock excitation no performance prediction methods were found. This is likely because most researchers focus on bistable energy harvesters, given the fact that interwell motion can be triggered by shocks.

Bistable Research has shown that bistable energy harvesters are sensitive to shocks [8][36]. The impulse of energy from a shock can create two types of dynamics: interwell and intrawell motion. As expected from the scaling of power with velocity squared, the interwell motion has the largest contribution to the total power: the harvested energy by the initial phase of snap-through motion is a magnitude larger than the intrawell cycles that follow snap-through motion [37]. Analytical models for bistable energy harvesters under shock conditions were commonly based on the averaging method. This had the consequence that these models would only describe small displacements from its equilibrium points. Harne therefore created a new analytical approach using the Jacobian elliptic functions, which describe the full electrical and mechanical dynamics including interwell motion [37]. The analytical model has two main sets of equations, one of which describes the displacement and velocities for interwell dynamics and the other for intrawell dynamics. The transduced voltage can be calculated from the time-dependent displacement and velocities. The type of dynamics (interwell vs. intrawell) is determined by the instantaneous energy of the system. The model of Harne was validated using both numerical and experimental tests where it was shown to be accurate. From Harne's paper no conclusions were made on how system parameters effect the power output, thus this is something to be investigated in future research.

2.8. Discussion

2.8.1. Limitations

Vibration types

Limitation of nonstationary vibration description - A distinction was made between nonstationary vibrations and band-limited noise. It is important to note however that the non-stationary vibration is described by gaussian modulated AM/FM signals. This type of non-stationary vibration does not describe all types of nonstationary vibrations. Furthermore, the PSDs for both types of vibrations will show a lot of similarities: there will be a frequency band with a relative high power and its surrounding frequencies will have low or almost no power. The band-limited noise will show a power that is attenuated more the further from the band-pass, whereas the nonstationary signal will show a near-constant power far from the central frequency. Still, these are different types of vibrations, in band-limited noise the frequencies in the band-pass exist all the time, whereas the surrounding frequencies in nonstationary vibration occur stochastically.

Vibration identification

Pre-conditioning data - An important sidenote is the effect of pre-conditioning measurement data on the visualization. Firstly, it is important to be aware of the limitations of the FFT and how to choose a proper window. Choosing no or the wrong window

will result in a loss of information or inaccurate information (for example detecting vs. not detecting shocks as described earlier). *Sensor noise* – It is important to consider (and possibly compensate) for sensor noise. When the noise levels are high relative to the vibration levels it may impact visualization of the actual vibration causing the user to identify the wrong type of vibration. Also, the sensor noise could affect the predicted output power since performance prediction methods assume that the entire signal power consists of kinetic energy.

Performance prediction

Classification of dynamics - The classification in this literature review was made for linear and nonlinear (monostable / bistable) energy harvesters. This is a general description that applies to a wide variety of energy harvester designs, but some designs will not fall in this category. Frequency-up conversion mechanisms that make use of plucking for example cannot be modelled with the methods in this paper. This is a result of the scope of this paper and thus something to be investigated at a later stage. *AC/DC-conversion* – When energy harvesters are used to charge batteries, the AC output of the piezoelectric material needs to be converted to DC. Converting the AC current to DC requires electrical rectifiers. The introduction of such a circuit introduces nonlinearity to the system. The methods in this paper make use of a resistive load which is linear, thus this limitation creates parasitic nonlinearity. Research by Zhang et al. showed that the AC circuits only add damping to the system, whereas AC/DC circuits add both damping and stiffness to the system [19]. *Coupling of parameters* – The analytical methods described in this paper make it possible to draw conclusions on how certain parameters affect performance. However, in practice it is not always possible to change one parameter without affecting others. This coupling of parameters will make the design cycle of an energy harvester harder in practice than it is on paper or in a simulation.

2.8.2. Future work

A complete overview of performance prediction methods could not be made. For some combinations of the types of vibrations and energy harvesters no methods were found. This is a clear gap for future research.

Nonlinearities considered in this paper are stiffness-nonlinearities. For future work it would also be interesting to investigate the effect of damping and inertia nonlinearities. So far, little work has been found about these types of nonlinearities.

2.9. Conclusion

Using literature about vibrations and energy harvesters six different types of vibrations were identified. It was found that the visualization methods power spectral density and spectrogram are best for identifying the types of vibration in a measurement. An overview was made of literature that discusses analytical performance prediction of the different types of vibrations for both linear, nonlinear monostable and nonlinear bistable energy harvesters. A summarized overview of all results can be found in section A.2. For the following combinations of energy harvester types and vibration types no analytical performance prediction methods were found: filtered noise linear, filtered noise nonlinear monostable, band-limited noise nonlinear and shocks nonlinear monostable.

It was found that nonlinear energy harvesters under noisy vibrations are generally modelled by calculating their PDF using the Fokker-Planck equation. Furthermore, it was found that the increased theoretical bandwidth of nonlinear energy harvesters does not always translate to a higher power output. Firstly, because high-energy orbits cannot be maintained for low excitation levels, and secondly because for a too high time constant ratio the nonlinearity will lower the power output.

3

Measurement setup & system identification

3.1. Measurement setup

3.1.1. Overview of measurement setup

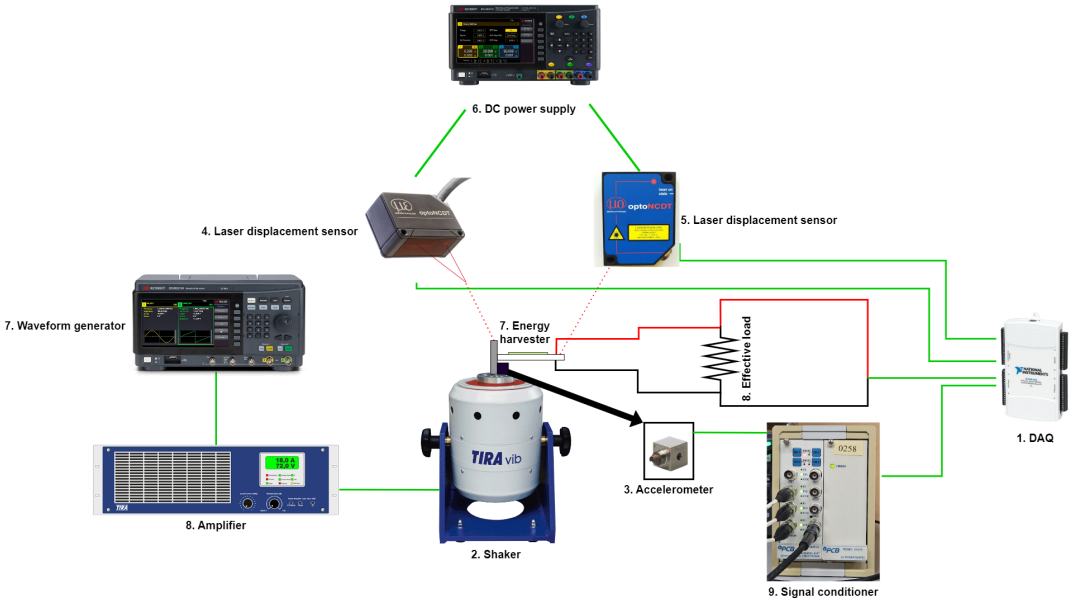


Figure 3.1: Wiring diagram of testing setup. Green lines indicate a pair of wires, and red and black lines indicate plus and minus, respectively.

Replication of vibrations is done using an electromagnetic shaker (TV51140). The energy harvester is mounted on the shaker and the output terminals of the piezoelectric transducer are connected to a resistive load. The voltage of the piezo is monitored over a load since the exact value of the load needs to be known to calculate the power accurately. Also, the power is dependent on the load; thus, during testing, it is needed to use different loads to find which one is optimal. Two types of electrical circuits are used for this. Type 1 has a fixed load, which is used to take accurate measurements, and type 2 has a variable resistance which is used to find the optimal load (more on this is discussed in subsection 3.1.2). The output voltages of these circuits are connected to a DAQ to calculate the power output.
The input displacement (displacement of the base of the shaker) and tip displacement are measured using a Micro-Epsilon optoNCDT1420 and optoNCDT1401, respectively. The acceleration of the shaker is monitored with a PCB 356b21 ICP accelerometer in combination with a PCB signal conditioner, model

441A101.
All inputs are connected to a central DAQ, which is the National Instruments USB-6211. The DAQ is connected to a laptop with Labview, which shows and logs the live data.
It is a good practice to keep all wires as short as possible and twist all pairs. This reduces noise and therefore gives better measurements.
A more detailed overview of the measurement setup, specifications and Labview interface can be found in Appendix B.

3.1.2. Power measurement

Fixed load (type 1)

When the optimal load is known, the instantaneous power can be calculated by monitoring the voltage across the load, where the voltage is determined as:

$$P_{load} = \frac{U_{load}^2}{R_{load}} \tag{3.1}$$

When the voltage across the load crosses the +/- 10 volts, a voltage divider is needed to make the



Figure 3.2: Simplest type of circuit that can be used to measure the power output of an energy harvester

voltage measurable and keep it within the limits of the DAQ. This voltage divider can be put in parallel with R_{opt}, or it is possible to put two resistors in series that together form the optimal load. If you measure the voltage across the smallest resistance, you measure a fraction of the total voltage.

Variable load (type 2)

If the optimal load is yet to be found, it is best to use a variable load to sweep through a series of resistances efficiently. This is done using a decade box. If one wants to see the change in instantaneous power directly, the power needs to be calculated independently of the load resistance. This is done with the circuit depicted in Figure 3.3 and with Equation 3.2.

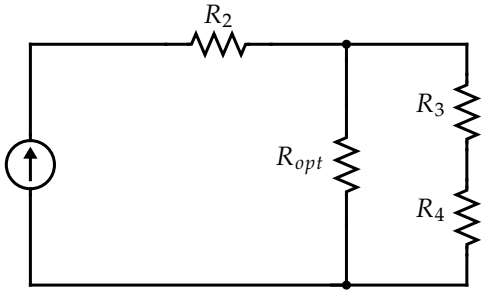


Figure 3.3: Electrical circuit that is used during load matching. The use of extra resistances makes it possible to calculate the power output independent of the load resistance. This allows for easy & fast tuning.

$$\begin{aligned} P_{load} &= U_{load} \cdot I_{load} \\ U_{load} &= \frac{U_4}{R4} \cdot (R3 + R4) \\ I_{load} &= \frac{U_2}{R_2} - \frac{U_4}{R_4} \end{aligned} \tag{3.2}$$

It is important to consider the fact that the load for the piezo is a combination of the load set on the decade box *and* the load of the resistances. Therefore, the total effective load is:

$$R_{load,eff} = R_2 + (\frac{1}{R_{load}} + \frac{1}{R_3 + R4})^{-1} \tag{3.3}$$

The pros of using this circuit is that one can directly see the effect of a change in the load on power output. When only using one resistance, one would have to manually calculate the power after a test, or you would have to adjust the value of the current load in Labview each time to see what the power is. This type of circuit is therefore not necessarily needed, but it speeds up the process of load matching and prevents errors that could happen in the data-processing.

3.1.3. Use of the shaker

System identification

Actuation of the shaker is done by sending a voltage signal from the signal generator to the amplifier, which is amplified and sent to the shaker as a current signal. To replicate vibrations one needs to compensate for the dynamics of the shaker. This is done by creating a transfer function of the current input to the shaker to the base acceleration, and use this relation to convert an acceleration profile to a current profile.

The shaker can be approximated as a mass-spring-damper system, which is described by:

$$m\ddot{x} + c\dot{x} + kx = F \tag{3.4}$$

In the frequency domain, this gives the transfer function of acceleration to current as:

$$TF_{acceleration/current} = \frac{s^2}{ms^2 + cs + k} \tag{3.5}$$

The effective moving mass is given by the supplier (see Figure B.3b). The transfer function is fitted and compared to the experimental data to check if they correspond.

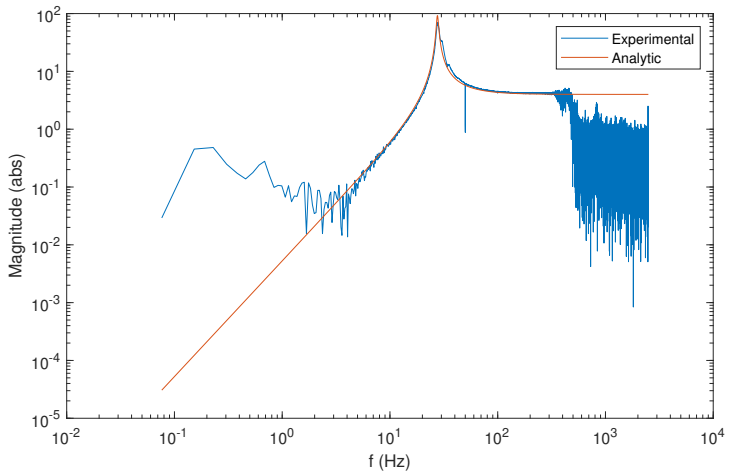


Figure 3.4: Combined plot of experimental and estimated transfer function to show that the estimated transfer function is valid.

It can be seen that the experimental and analytic functions overlap from 1 Hz up to approx. 500 Hz, which covers the whole range of frequencies that need to be reproduced in this research.

Converting vibration profile to current profile

When you have a vibration signal in your Matlab workspace, and the transfer function from current to acceleration is known, it is easiest to use the Matlab function *lsim(sys,u,t)* to convert the vibration to a

current profile. This function calculates the response of a time-domain signal to a given system *sys*. If you input the vibration u, and the inverse of the transfer function, it returns the current signal.
When performing slow frequency sweeps this approach yields good results for replicating an acceleration profile. Because at each time instance there is only one, or a few, frequencies; and they are filtered out according to the magnification at those particular frequencies. However, if you want to replicate more complex signals, such as real-life vibrations with non-stationary frequencies, this approach will not yield an accurate acceleration profile. The fast dynamics will still actuate the eigenmode of the shaker since the fitted profile does not exactly overlap with the actual transfer function.

Decreasing the natural frequency and improving stability
From the signal identification in Figure 3.4, two things can be concluded. First, one needs a high gain when operating the shaker below its natural frequency. And second, above resonance the frequency response has a constant gain, thus is easy to control the shaker.
When performing experiments at low frequency and moderately high acceleration, it is therefore hard to achieve a constant acceleration. Therefore, a mass is added to the shaker. This lowers the natural frequency, making it easier to produce low-frequency vibrations, and the increased inertia will make the system less sensitive to disturbances. This is especially needed for testing bistable energy harvesters, where the reactive force of snap-through motion will affect the acceleration if the fixed mass is low relative to the reactive force of the harvester.

The Tira TV51140 is tested with a maximum weight of 6 kilograms. Therefore, the total system mass should stay below 6 kg. The effective moving mass of the internals of the shaker is 0.4kg, and most test objects weigh up to 1kg. So, the mass to be added to the shaker should have a maximum weight of 4.6kg.
Two circular steel disks are produced that can be mounted on the shaker, each weighing approximately. 2.25kg. The disks are bolted to the top of the shaker and the mounting holes on the steel disks have the same dimensions as the shaker top, which makes it possible to mount existing designs.



Figure 3.5: Shaker mass mounted on the shaker.

3.2. System identification

This research tests two energy harvesters: a piezoelectric cantilever and bistable buckled beam. Before conducting the actual tests, a system identification is performed for both harvesters to determine the system parameters experimentally. These system parameters will be used as inputs to the model. Also, the system identification will give information about the regimes in which the harvesters operate, which

is used to compose the test vibration signal (see paper). The steps of the system identification are visualized in Figure 3.6.

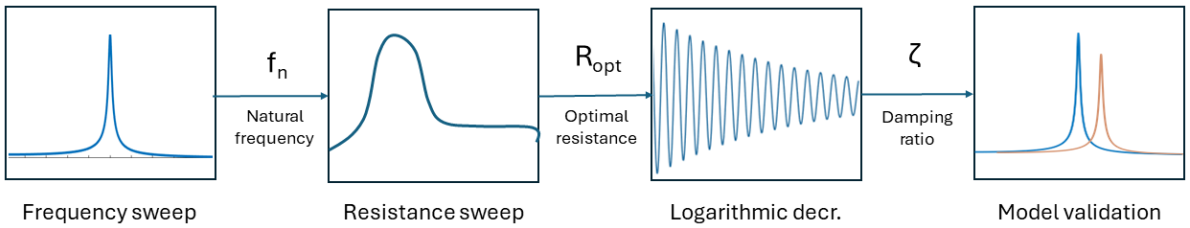


Figure 3.6: Visualization of the steps that are performed for the system identification and model validation, which are performed *before* the double frequency tests are performed.

3.2.1. Piezoelectric cantilever

Natural frequency

The natural frequency of the cantilever is determined first. By doing a frequency sweep and monitoring the tip-deflection, the natural frequency is found at the frequency where the deflection is maximum. It was found that the natural frequency of the cantilever is 87 Hz.

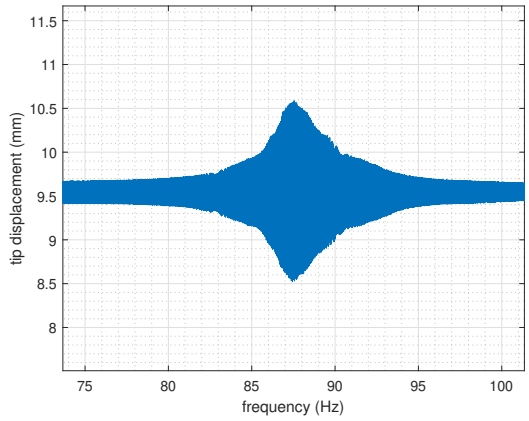


Figure 3.7: Tip displacement of the cantilever when subjected to a frequency sweep. The plot is zoomed to the resonance regime. The frequency sweep is performed with the optimal load attached. Deflection is maximal at 87 Hz, so this is the experimental eigenfrequency of the cantilever.

Resistance sweep

To make a fair comparison between experimental and theoretical power output a resistance sweep is performed to find the optimal load. This is done by using a decade box, i.e. a number of variable resistance that are connected in series, where each variable resistance spans one decade (for example from 10Ω to 100Ω). By increasing the resistance stepwise, the power will increase until the optimal load, after it will drop down. The point where the highest peak power is measured, is considered as the optimal load and this will be used for the rest of the measurements.
Since the optimal load is dependent on the electrical frequency of the system, the resistance sweep is performed at the mechanical natural frequency of the system of 87 Hz. It was found that the optimal load at this frequency is 14500 Ω.

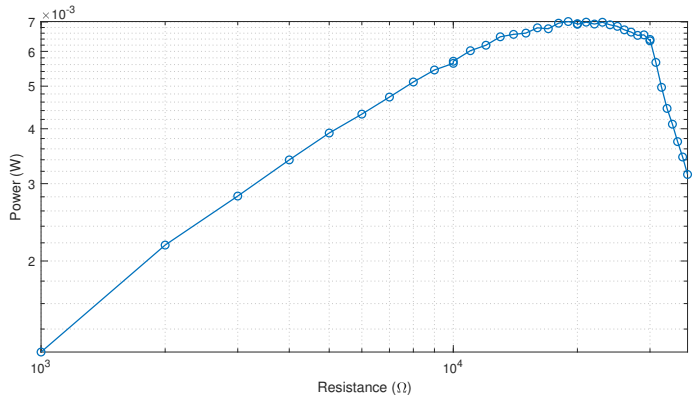


Figure 3.8: Electrical power output of the cantilever energy harvester across different loads measured at constant acceleration. Stepsize is 1000 Ω.

Damping ratio

The damping that is needed as an input for the model is the mechanical damping of the system. Therefore this is measured while the cantilever is clamped on the shaker and the terminals of the piezo are short-circuited. While keeping the shaker turned off, the tip of the cantilever is excited by tapping it, and the deflection is measured afterwards. The damping ratio ζ is then calculated using the logarithmic decrement method:

$$\begin{aligned} \delta &= \frac{1}{n} \log \frac{x(t)}{x(t+nT)} \\ \zeta &= \frac{\delta}{\sqrt{4\pi^2 + \delta^2}} \end{aligned} \tag{3.6}$$

Using this method, the damping ratio was found to be 0.01428.

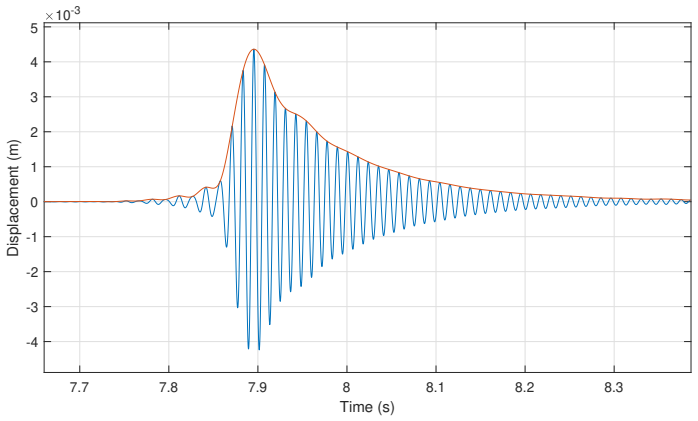


Figure 3.9: Fading out of the displacement over time, after tapping the tip of the cantilever. From the measurement, the damping ratio was found to be 0.01428.

Model validation

This section aims to validate the model used for simulating the piezoelectric cantilever proposed by Sodano et al. [38] before using it in the paper. This is done by comparing the analytical and experimental power profiles and check their correspondence. Therefore, an experimental frequency sweep is performed first, with the optimal load to create the experimental power profile.
Next, the power profile is calculated with the model. However, the analytical model assumes a fully covered bimorph cantilever, while the test object is an unimorph partially covered cantilever. Therefore the power is overestimated if not adjusted for it. By introducing a fitting parameter, the analytical power curve is fit to match the experimental power profile. Figure 3.10 shows that experimental and

analytical power profiles overlap for the measured system parameters after applying a fitting parameter which scales down the total power by a factor of 0.23. (more details about the fitting can be found in Appendix D). Therefore, the model and its implementation are correct and can be used for the double frequency tests.

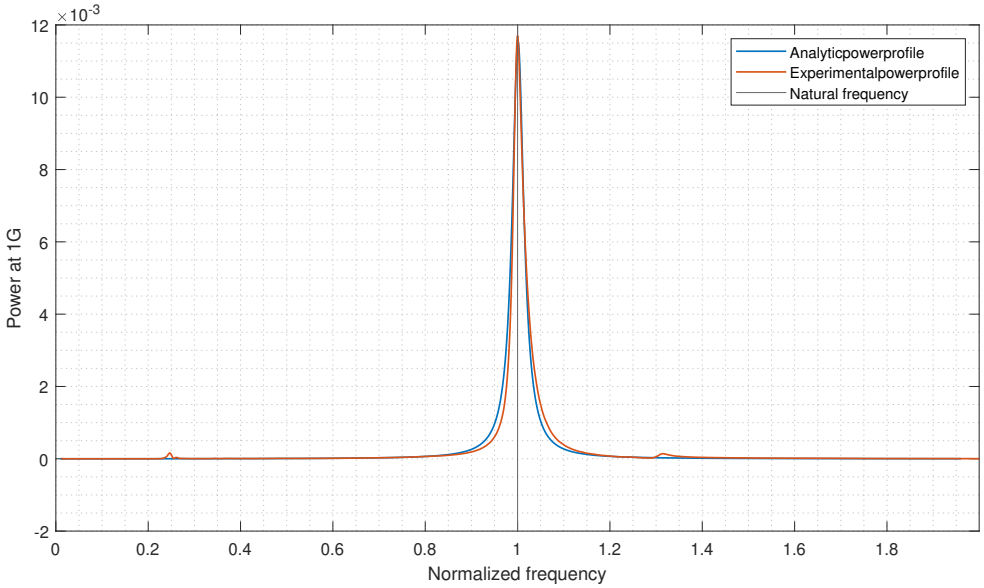


Figure 3.10: Experimental and analytical power profile at 1G, normalized to the eigenfrequency of the system. The plot shows that there is good correspondence between the profiles. The peak power at resonance matches and the bandwidth also shows close resemblence.

3.2.2. Bistable energy harvester

Force deflection measurement

The force-deflection curve is measured to determine the potential function which is an input to the numerical model. A NEMA 11 stepper motor is combined with a TB6600 micro stepper driver, which actuates a linear guided spindle. A Mavin NS7-10KG load cell is used to measure the reactive force. An extra proof mass is attached to the flexure during the test to make the system monostable. By doing this, the measured force is always of the same sign; this means there is no snap-through motion and the measurement is more accurate since there are no dynamics. After the measurement, the known mass is subtracted from the force profile to get the proper force deflection of the energy harvester.

The force-deflection profile is measured forwards and backwards. A proof mass of 110.5 grams is used, and the force-sensor has a static offset of 2.1 N. After substracting these from the measurement, a 4th order polynomial is fit to the curve:

$$F(x) = p_1 x^4 + p_2 x^3 + p_3 x^2 + p_4 x + p_5 \tag{3.7}$$

p_1	-2.711e08
p_2	-7.061e06
p_3	2.073e05
p_4	-1108
p_5	0.8382

Table 3.1: Weights of the polynomial that describes the force-deflection profile

Fitting was done using the Matlab fitting toolbox. The fitted profile will be used as an input for the

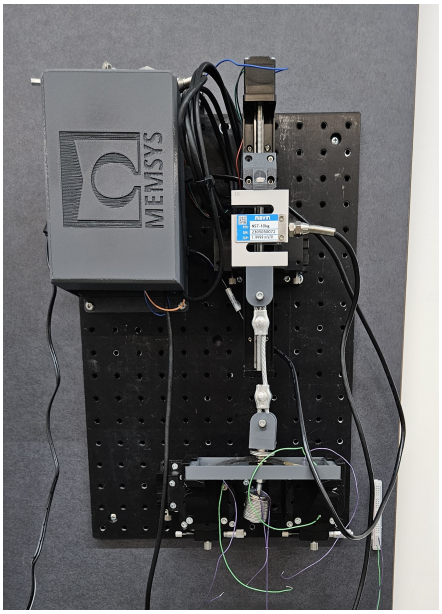


Figure 3.11: Setup used for measuring the force deflection profile. Note that the setup is hanging on the wall, so that gravity is acting on the mass.

numerical model of the bistable harvester. Figure 3.12 shows the measured data and fitted polynomial of the force-deflection.

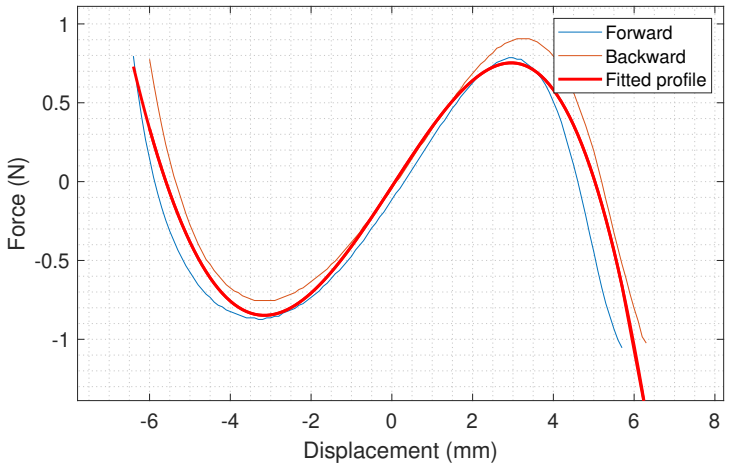


Figure 3.12: Force-deflection curve of the bistable energy harvester. The curves have a vertical offset due to an attached mass that is added during the measurement, in order to prevent a fast snap-through.

Figure 3.12 shows the reaction force from the flexure. When mounted in the casing there will also be a static force from gravity. The effect of this force is best visualized using the potential energy curve:

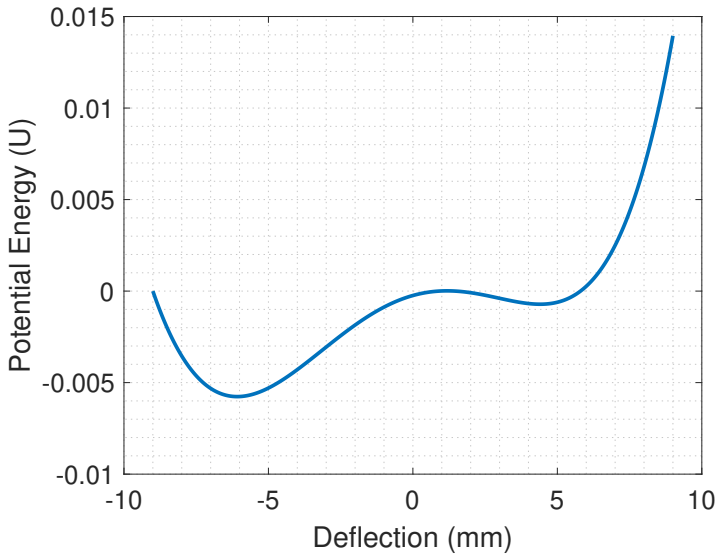


Figure 3.13: Potential energy curve, showing the potential energy in the system as a result of deflection of the spring and work from gravity. Note that the profile is asymmetric due to gravity.

Figure 3.13 shows the asymmetry in the potential curve of the bistable harvester due to gravity. The unequal equilibrium points show that it is easier for the system to switch from the high to low equilibrium state (right to left), than from the low to high equilibirum (left to right). Therefore, it can be expected that the system has a preferred equilibrium position if the excitation signal does not input enough energy to span the largest energy gap.

Resistance sweep

The optimal load of the energy harvester has to be found before conducting the power measurements. The operating modes of the bistable energy harvester can be subdivided into intrawell motion, interwell motion and a mix of both. Since the interwell motion is able to harvest the most power, the load resistance is tuned for this operating mode (check chapter 2 for more information about these modes). Also, the load resistance will be used as an input to the numerical model.
The load matching was conducted with a fixed acceleration level that is sufficient to maintain the interwell motion. Figure 3.14 shows that the optimal load is approximately $115k\Omega$, thus this load resistance is used in the experiments.

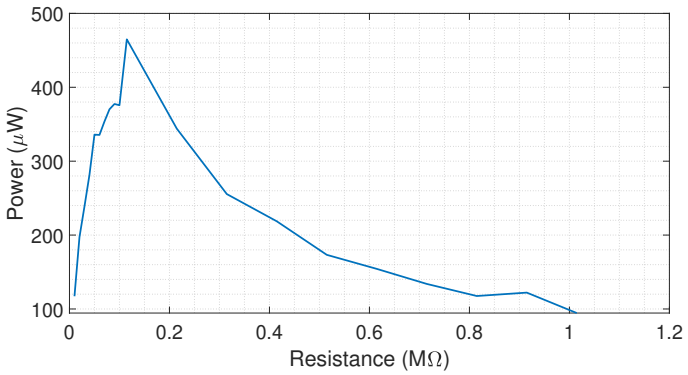


Figure 3.14: Plot of power vs. resistance to determine the optimal load of the bistable energy harvester during interwell motion

Damping coefficient

The mechanical damping coefficient is measured since it is an input to the numerical model. The logarithmic decrement method is used to back-calculate the damping coefficient. However, the absolute

displacement is kept really small so that the harvester moves in its linear regime.
The laser sensor was not available at this time of the research. Therefore, the voltage of the piezo is monitored to determine the damping; this is valid since the voltage is linearly related to the stress, and the harvester is moving in its linear regime. The damping coefficient was found to be 0.2329 Ns/m.

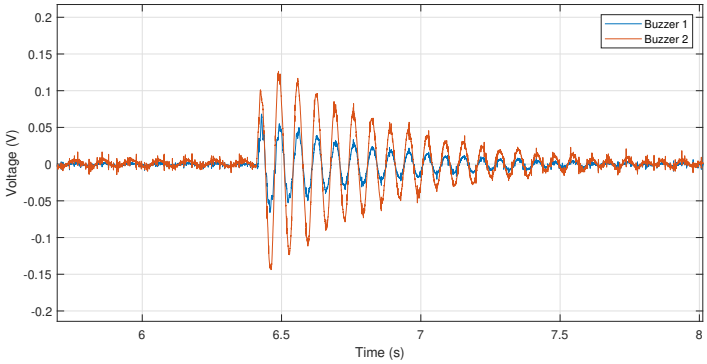


Figure 3.15: Fading out of the voltages over time, after tapping the mass. From the measurement the damping coefficient was found to be 0.2329 Ns/m.

Electromechancial coupling coefficient

The electromechanical coupling coefficient is calculated by exciting the harvester at a constant harmonic acceleration, monitoring the voltage and then fitting the coefficient for the voltage in the numerical model. From this, it was found that the coefficient is 0.00024 N/V.

Optimal frequency

First, the frequency at which the harvester generates the highest power is identified using a frequency sweep; this frequency is needed since it will be kept constant during the double-frequency test. To identify the high- and low-energy orbits of the system, a frequency up- and frequency downsweep are performed.

4 frequency sweeps are performed experimentally, each with different amplitudes. The frequency sweeps run from 13-30 Hz (upsweep) and 30-13 Hz (downsweep) in 60 seconds. The power is monitored over the optimal load of 115kΩ.
From Figure 3.16 it can be concluded that the energy harvester is most efficient in the range from approx. 20-26 Hz for the tested signals. Also, the harvester shows a softening effect. The downsweep shows a large bandwidth, since the harvester can maintain a fixed orbit, whereas for the upsweep the power profiles show a sudden jump and large variations in power, which could be an indication of switching between interwell and intrawell motion.
It is worthwhile to point out that during the downsweep, the resonance frequency decreases for lower excitation levels, and the bandwidth increases for lower excitation levels. Also, the peak power for each excitation level is quite similar: approximately $240 - 260\mu W$.
From the frequency up- and downsweeps 23 Hz at 1 G is selected as the most optimal frequency. This vibration lies approximately in the middle of the different frequency responses for the frequency upsweep and it harvests a substantial amount of power. For the frequency downsweep it will not generate the highest absolute amount of power, but it will harvest power over a larger range of excitation levels.

Model validation

This section aims to validate the numerical model proposed by Daqaq et al. used for simulating the bistable energy harvester before using it in the paper [8]. The model is validated by simulating the harvester for the frequency sweeps performed in the preceding subsection and comparing it with the experimental data. Starting with the frequency upsweep, it can be seen in Figure 3.17 that the simulation shows a softening behavior, which was also seen in the experiment. The sweep with an amplitude of 1.3 G generated so much power that it could not be plotted on the same scale. After further inspection, the simulated displacement data for A = 1.3 G showed that the dynamics of the harvester are valid: the

harvester is constantly snapping through, but its maximum displacement is close to its stable points. This magnified power was also seen during the experiment; however, the orbit could only be maintained up to approx. 15 Hz. Furthermore, comparing the power profiles of 1.08 G from the simulation and the experiment, the simulated profile is much smoother.
Because of the softening behavior, the downsweep has a greater bandwidth than the frequency upsweeps. However, the increase in natural frequency that was seen for an increase in amplitude during the experiments, is not seen in the simulation. The simulated data shows a decrease in natural frequency when comparing 0.24 G to 0.53 G, and thereafter an increase when comparing 0.53 G to 0.92 G.
Overall, the experimental and simulated frequency sweeps show acceptable correspondence. Thus the implementation of model is correct, and therefore the model can be used for the double frequency tests.

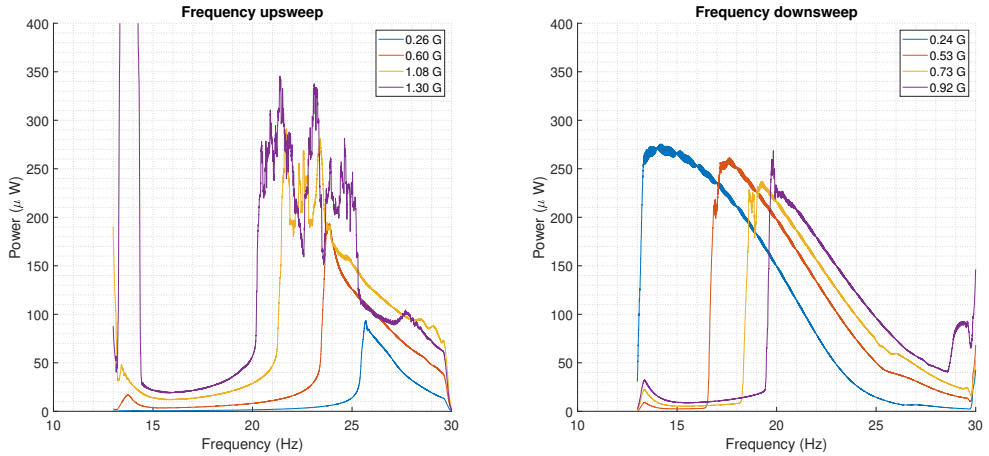


Figure 3.16: Moving average of the experimental power during the frequency sweep. Time window of the average power is 1 second. The peak at 1.3 G acceleration (that lies out of the plot) during the upsweep reaches 1100μW.

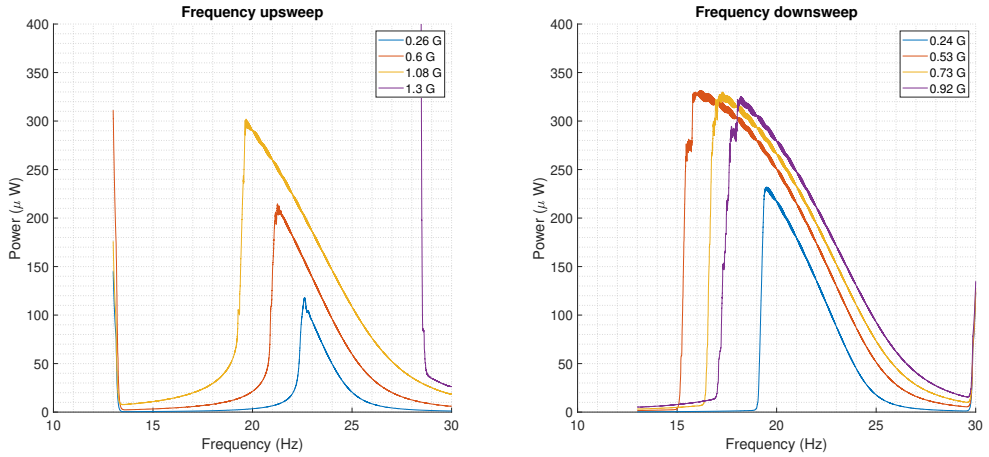


Figure 3.17: Moving average of the simulated power during the frequency sweep. Time window of the average power is 1 second. The peak at 1.3 G acceleration (that lies out of the plot) during the upsweep starts at 1000μW at 13 Hz, and reaches 4600μW at 28 Hz.

3.3. Train vibrations

The first step in creating an energy harvester for train sensors is analyzing and understanding the characteristics of train vibrations. This section contains an overview of the analysis of train vibrations. To narrow the scope, a section of vibration data of a freight train driving at a constant speed is analyzed. This section is chosen because train vibrations will likely be most predictable when driving at a higher

constant speed, compared to a train moving slowly on a freight yard. Thus, it is easiest to design a harvester for this case. Also, it will likely result in the most amount of net-harvested energy because a train spends most of its time traveling on long rail tracks.

Three methods are used to visualize the train vibrations and find their properties:

I. Fast fourier transform
A Fourier transform shows that the vibration power is quite flat, with some dominant frequencies: 4 dominant vibrations in the range from 25-65 Hz and 1 dominant frequency at 283 Hz. Although the high-frequency vibration has a large acceleration amplitude, it is not considered to harvest energy from this vibration due to its low displacement. Also, the high-frequency vibration does not reoccur in every dataset; thus, it is questionable whether this peak is reliable.

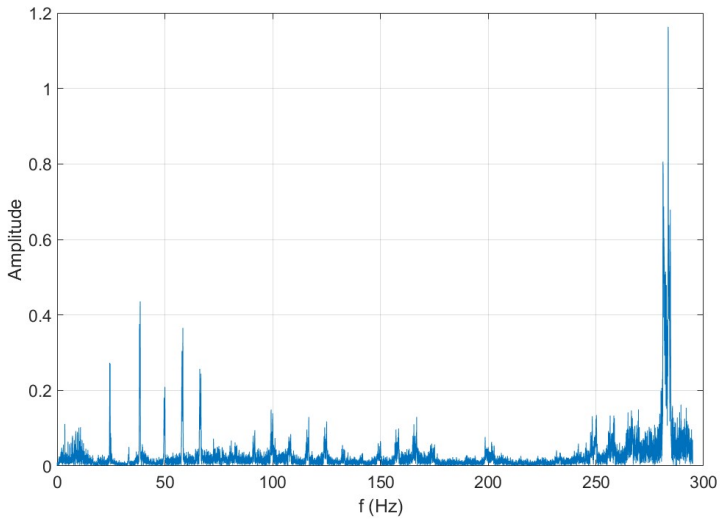


Figure 3.18: Fourier transform of the vibrations measured on a freight train driving at a constant speed.

II. Spectrogram
The spectrogram shows that these dominant vibrations are constant over time: their frequency stays constant, and the vibrations is also always existent. This is important information since it means that an energy harvester can be designed for a specific (set of) frequencies and that it then should harvest energy almost continuously while driving.

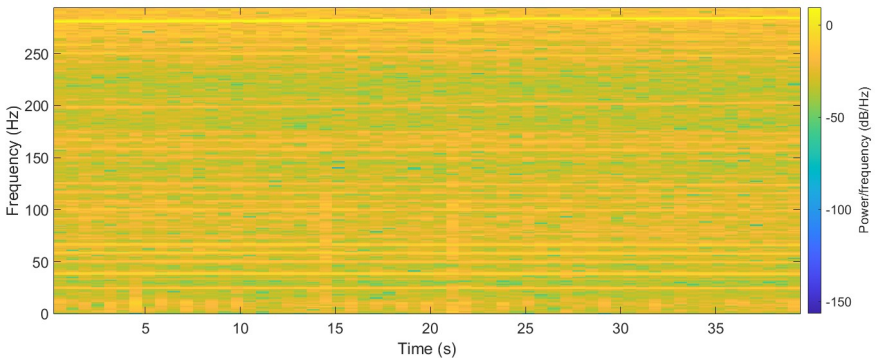


Figure 3.19: Spectrogram of the vibrations measured on a freight train driving at a constant speed.

III. Time-domain data
Lastly, the time-domain data shows the effect of the multiple dominant vibrations that are closely spaced together in the range of 25-65 Hz: the different frequencies interfere, and a beating effect occurs: although the different frequencies are constant, they interfere over time, causing the amplitude of the vibration to be not constant.

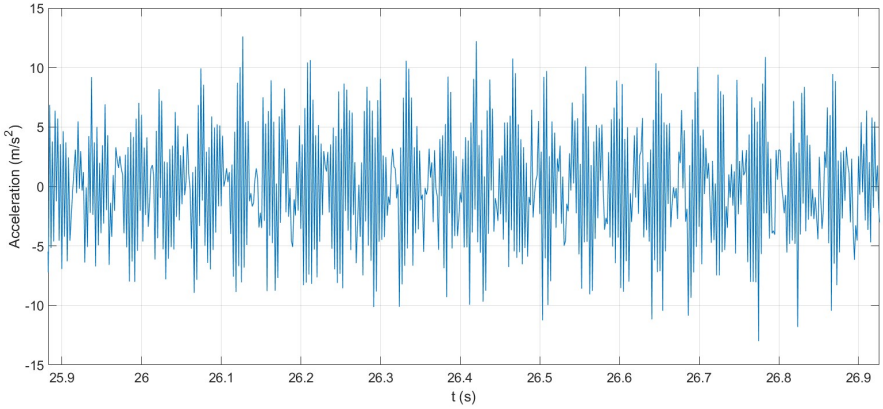


Figure 3.20: Plot showing 1 second of the vibration data measured on a freight train driving at a constant speed.

This analysis shows that a train vibration's acceleration profile is constantly changing due to interference between coexisting harmonic frequencies.
This beating effect occurs when two or more frequencies are added together. Therefore, the research replicated this phenomenon by adding two frequencies and changing the amplitude and frequency spacing.

4

Effect of multi-frequency vibrations on energy harvester power output and theoretical predictability

"In theory, theory and practice are the same. In practice, they are not."

Albert Einstein

Effect of multi-frequency vibrations on energy harvester power output and theoretical predictability

J.P. Verduijn, Wednesday 18th September, 2024

Abstract - This paper tests the effect of multi-frequency vibrations on the power output of piezoelectric energy harvesters. These tests were conducted to show how the output power scales when an energy harvester is excited not only at its eigenfrequency, but also at an off-resonance frequency and how well theoretical models predict power output under these conditions. A linear cantilever and bistable buckled beam are tested experimentally on an electrodynamic shaker and simulated using existing models to compare the accuracy of these models under such excitations. The excitation signal has one fixed frequency component, which matches the eigenfrequency of the energy harvester; and a second vibration component, which has a frequency and amplitude that are varied. For a linear cantilever, it was shown that an existing closed-parameter model can predict power output for the mechanical and electrical parameters, where the power is a summation of the power generated by each separate frequency. However, even a simple cantilever shows nonlinearity for high excitations; this is something one needs to account for if you use the model to calculate expected power output. For a nonlinear harvester it was shown that the power output scales linear with the amplitude of vibration when subjected to a single sine. For multi-sine vibrations, the power output is only slightly increased by adding the second frequency, indicating that the beneficial bandwidth of a nonlinear energy harvester is much smaller when absorbing energy from a second frequency.

4.1. Introduction

Vibrational energy harvesting is a promising solution to power wireless sensors. When implemented successfully, sensors can be powered infinitely without the need to replace batteries. This is attractive from a financial point of view, as well from sustainability, since it prevents battery waste. Moving vehicles have a great potential for this technology; these large moving assets contain a high amount of kinetic energy, and other energy harvesting solutions such as solar power are not viable in the long term due to dirt and dust.

The first vibrational energy harvester designs were based on resonance. Their output power is high when excited at their eigenfrequency (4mW at 0.65 G), but due to their low bandwidth the output power in real-life remains too limited to power a sensor. Research is therefore moving to nonlinear energy harvesters, which have a higher bandwidth. But still no real-life cases have been found. This indicates there remains a gap between the power that is expected when tested in a lab, versus the power that is actually harvested when the device is mounted on a vehicle. This paper focuses on this mismatch in power to better understand and design energy harvesters that can power wireless sensors.

From the analysis of train vibrations, it was found that the vibration power spectrum of these vehicles is often characterized by multiple dominant frequencies. Up to now, research has tested energy harvester performance with frequency sweeps or (colored) noise. It is not clear if these tests are still accurate when the harvester is subjected to multiple dominant vibrations at the same time. Therefore, this study is the next step in testing energy harvester performance for vibrations that one will encounter on trains, and it will establish a basis for understanding the applicability of existing models and performance metrics to these environments.

This is done by studying the effect of interference between two dominant vibrations on the power output of piezoelectric energy harvesters. The power output is calculated using a theoretical model and compared with the experimental results. This comparison gives insight into the impact of multi-frequency vibrations on power output, as well as how accurate theoretical models and simulations can capture this effect.

If the theoretical models can accurately predict the power output for multi-frequency vibrations, these models can be used to optimize designs for specific excitation signals, which eventually could translate into different designs for different types of trains.

Also, it will show if single-sine frequency sweeps that are often presented in design papers are representative for environments with multi-frequency vibrations or to what extent they can predict the power output.

Section 4.2 contains an overview of the methods that are used to come to the results presented in this paper. It covers the designs and parameters of the tested energy harvesters, the specifications of the test setup, a breakdown of the vibration signal that is used to test the energy harvesters, the theoretical models to simulate the energy harvesters and finally the testing procedures. Section 4.3 presents the results, which show the influence of a multi-frequency signal on the power output. Section 4.4 contains the discussion, where the results are interpreted. Finally, the main conclusions are summarized in section 4.5.

4.2. Methods

Two energy harvesters are tested in this research: a unimorph cantilever and a bistable buckled cantilever. A cantilever is chosen because of its simplicity and excellent performance at resonance. In theory, a cantilever is a linear system. According to the linearity principle the total power is therefore the sum of the power of each frequency. This paper tests if the linearity principle can indeed be extended to a cantilever energy harvester when subjected to two dominant frequencies and it sets a baseline of the linearity principle.
The second prototype, a bistable buckled beam energy harvester, is tested because of its promising wide bandwidth and ability to harvest energy from shocks while being more sensitive to a change in input vibrations because of its nonlinearity and, therefore, being less predictable.

4.2.1. Dynamic test setup

The energy harvesters are tested in a lab setting using a Tira TV51140 electrodynamic shaker. The acceleration is monitored using a PCB35621 piezo accelerometer, which is connected to a PCB signal conditioner and logged by a NI USB 6211 Data Aquisition System (DAQ). The power output of the energy harvesters is measured over a pure resistive load, of which the voltage is also logged using the DAQ.
During the experiments all outputs are logged and visualized using Labview.

4.2.2. Energy harvester design

Linear unimorph cantilever

A design from PI Ceramics is used as the test object for the piezoelectric cantilever. The design is part of the E-821 Piezoelectric Energy Harvesting Evaluation Kit. The energy harvester consists of a 1.3 mm thick carbon fiber substrate with a piezoelectric patch glued to one side. The piezoelectric material is of the type PIC 255. The design can be found in Figure 4.1 and the parameters in Table 4.1. The cantilever is mounted on the shaker with a milled clamp from aluminum. The clamped part of the cantilever is 20 mm long to ensure that the substrate is fully fixed.
The piezoelectric cantilever has an eigenfrequency of 87 Hz, a damping ratio of 0.01428, and at resonance, the optimal load is 17500 Ohms.



Figure 4.1: Piezoelectric cantilever from PI ceramics. Brown indicates piezoelectric material, and black indicates the carbon fiber substrate.

Cantilever properties	
Substrate	
Length (l_s)	130mm
Width (w_s)	35.0mm
Thickness (t_s)	1.30mm
Density (ρ_s)	2000kg/m^3
Modulus of elasticity (c_s)	200GPa
Piezoelectric patch	
Length(l_p)	61.0mm
Width (w_p)	30.0mm
Thickness (t_p)	0.50mm
Density (ρ_p)	7800kg/m^3
Modulus of elasticity (c_p)	62.0GPa
Dielectric constant (K_{3T})	1800ϵ_0
Piezoelec. coupling coeff. (d_{31})	−180pC/N

Table 4.1: Mechanical and electrical properties of the PI piezoelectric cantilever.

Bistable buckled beam

For the bistable design, a clamped-clamped buckled beam is used. The substrate consists of laser-cut 0.250 mm spring steel. An effective mass of 41.8 grams is attached to the center of the flexure to increase the input force from the external acceleration and make the harvester bistable under gravity (thus the mass oscillates in the z-direction).
Piezoelectric buzzers are used as transducers. After sanding and degreasing the surfaces, two buzzers are glued to the flexure, one per side (using AP Universal EP epoxy). The substrate of the buzzers is cut to the same width as the flexure. Each transducer is monitored separately for power measurements since connecting the terminals together could cause charge cancellation if the stresses are not the same sign.
The bistable mechanism has a bandwidth of approximately 20-26 Hz, a damping coefficient of 0.2329 Ns/m, an optimal load of 115 kΩ per buzzer for interwell motion, and an electromechanical coupling coefficient of 0.00024 N/V. The force-deflection profile of the flexure is described in Equation 4.1 and is visualized in Figure 4.4.

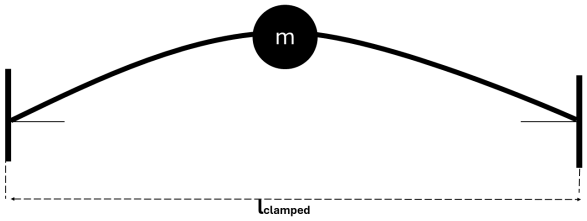


Figure 4.2: Schematic side view of the bistable energy harvester. A point mass is attached to the middle with a bolt and rings. The ends are clamped.

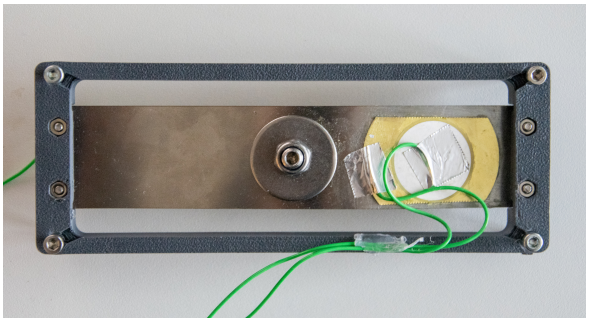


Figure 4.3: Topview of bistable energy harvester. The flexure is compressed in a 3D-printed casing. Piezoelectric buzzers are epoxied to both sides.

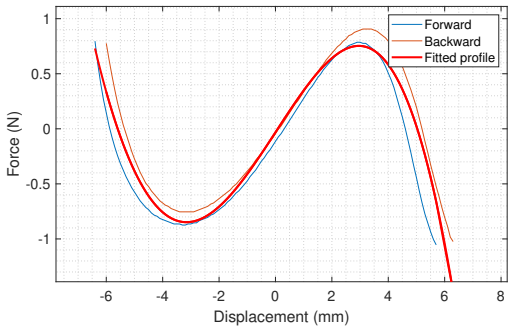


Figure 4.4: Force deflection profile of the buckled beam in the bistable energy harvester.

$$F(x) = -2.711e08x^4 + -7.061e06x^3 + 2.073e05x^2 + -1108x + 0.8382 \quad (4.1)$$

Bistable buckled beam properties	
Flexure dimensions	
Length ($l_{flexure}$)	142mm
Clamped length ($l_{clamped}$)	142mm
Width (w)	30mm
Thickness (t)	0.25mm
Proof mass (m)	48gram
Piezoelectric buzzer	
Diameter piezo (d_p)	26.0mm
Diameter substrate (d_s)	41.0mm
Thickness piezo (t_p)	89.2μm
Thickness substrate (t_s)	98.2μm
Capacitance (C)	78.5 nF

Table 4.2: Mechanical and electrical properties of the bistable buckled beam energy harvester.

4.2.3. Test vibrations

To test the effect of double dominant vibrations on the power output, a discrete frequency sweep with two frequencies is used; one frequency is fixed at the natural frequency of the harvester, and the other frequency is swept from below to above the natural frequency of the harvester. These two different frequencies will interfere with each other over time, creating a nonconstant amplitude that approximates the patterns that were identified on a railroad vehicle. A description of this vibration is

$$A(t) = A1 \cdot sin(2\pi f_1 t) + A2 \cdot sin(2\pi f_2 t) \quad (4.2)$$

Where A is the acceleration profile, A_1 and f_1 are the amplitude and the frequency of the fixed vibration respectively and A_2 and f_2 are the amplitude and frequency of the off-resonance vibration respectively. The motivation for this vibration profile is that an energy harvester is often designed

for the most dominant frequency. Therefore, one frequency is held constant at the mechanical eigenfrequency to represent the frequency for which the energy harvester is designed. The other frequency is one that the energy harvester is not designed for, but it is there in real life and, therefore, could affect the power output; which is this research about.
Since dominant real-world vibrations will have different amplitudes, the ratio A2/A1 is varied to give a fair comparison of the effect of the second frequency for real-world scenarios. The ratios tested are [0.2, 0.4, 0.6, 0.8, 1.0].
For the experiment, multiple tests are combined to produce one measurement. Per measurement, the ratio is fixed, and the frequencies vary step-wise. Each frequency is held constant until the shaker reaches a steady state. The energy harvester power output is then measured in the part where the shaker excitation is constant.
This 'discrete frequency sweep' is chosen to capture the beating effect accurately. A continuous frequency sweep would cause the spacing between the two frequencies to vary over time, thus also changing the beating period over time; which makes it impossible to capture a beating period associated with a constant frequency spacing. More information about the beating can be found in *Time domain visualization*.

Frequency domain visualization

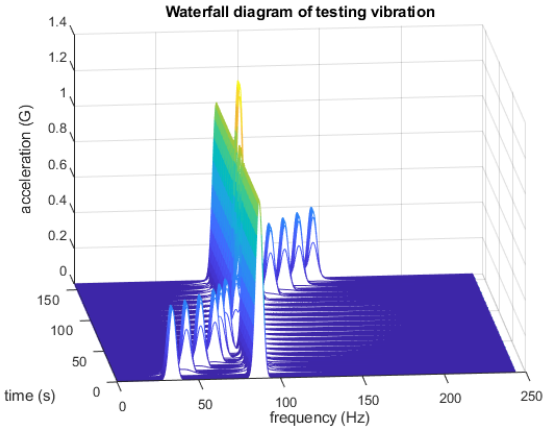


Figure 4.5: Waterfall diagram showing the test vibration described in Equation 4.2. For this case, f_n is fixed at 87 Hz, and f_2 is varied from 34 Hz - 145 Hz. The ratio between the amplitudes of both frequencies in this example is 0.4.

A short-time Fourier transform (STFT) of the test vibration signal visualizes how the frequency content changes over time during the experiment. An example is shown in Figure 4.5, where each frequency is held constant for 8 seconds. The total testing signal contains 20 frequencies.

Time domain visualization

One can see in Figure 4.6 that a beating pattern occurs when the two frequencies approach each other, where the maximum amplitude increases, but the amplitude will rise and fall over time.

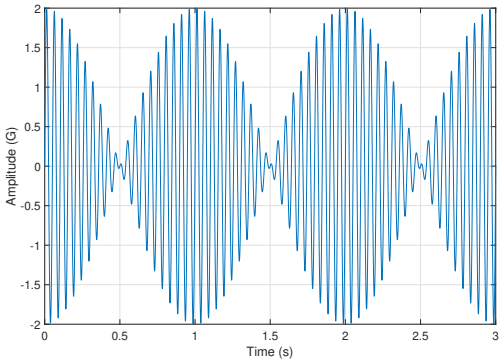


Figure 4.6: Summation of two sine waves to visualize the effect of beating. The first sine has an amplitude of A = 1 and a frequency of f = 20 Hz; the second sine has an amplitude of A = 1 and a frequency of f = 19 Hz.

An example of this is shown in Figure 4.7, where an energy harvester is modeled as a spring mass damper system subjected to base excitation. The plot shows that the energy harvester needs some time to build to its maximum deflection. The time before the steady state is reached is typically indicated by the time constant τ (Equation 4.3). A rule of thumb is that a system reaches its steady state in typically 5 time-constant periods [39].

$$\tau = \frac{1}{\zeta \omega_n} \tag{4.3}$$

The beating can be described by a carrier and envelope wave, which are described by

$$vibration = \cos(2\pi f_1 t) + \cos(2\pi f_2 t) = 2\left[\cos(2\pi \frac{f_1 + f_2}{2} t)\right]_{carrier} \cdot \left[cos(2\pi \frac{f_1 - f_2}{2} t)\right]_{envelope} \tag{4.4}$$

So, when $\Delta f = 1$, the envelope frequency of the vibration will be 0.5 Hz, and it takes 0.5 seconds to go from pure anti-resonance to resonance. Thus it is interesting to see how the beating affects the output power when $5\tau > \frac{1}{2\Delta f}$, since then the time response of the system is larger than the time it takes to go from pure anti-resonance to pure resonance.

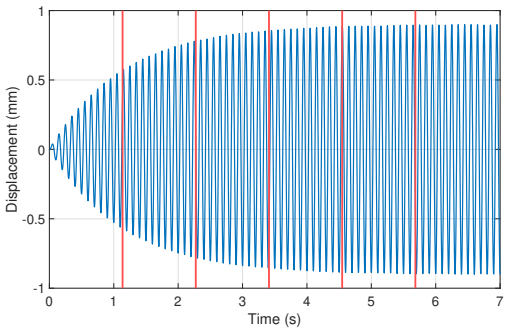


Figure 4.7: Transition of transient to steady-state of a spring mass damper system, with a damping ratio of 0.014. The blue line is the displacement of the mass, and the black lines indicate an integer amount of time constants τ.

4.2.4. Analytical model of piezoelectric cantilever

VEHs are commonly modeled as SDOF spring damper systems, where power conversion from the electric to the mechancial domain is modeled as velocity-dependent damping. Although this is accurate for magnet/coil transducers, it is not for piezoelectric transducers - as pointed out by Erturk et al. [21]. Therefore, the model from Sodano et al. is chosen, which captures the piezoelectric backward coupling and gives a fully closed solution for the output power for mechanical and electrical design parameters [40].
With this model, the dynamics are described by:

$$\begin{aligned}&(M_s + M_p)\ddot{r}(t) + C\dot{r}(t) + (K_s + K_p)r(t) - HC_p^{-1}q(t)\\ &= \sum_{i=1}^{n_f} \phi(x_i)^T f_i(t)\\ &R\dot{q}(t) - C_p^{-1}H^T r(t) + C_p^{-1}q(t) = 0\end{aligned} \tag{4.5}$$

Where $r(t)$ the temporal coordinate of the displacement, $q(t)$ is the charge, M is the mass matrix, C is the mechanical damping, K is the stiffness matrix, H is the electromechanical coupling, C_p is the capacitance matrix, ϕ is the mode shape function and $f(t)$ is the forcing function; the subscripts s and p indicate *substrate* and *piezoelectric* material respectively. Using Equation 4.6 the theoretical peak power for sinusoidal excitation is calculated as:

$$P = \frac{D^2A^2}{\sqrt{KM}} \times \frac{k^2r^2\lambda}{((1-r^2) - (2\zeta r^2\lambda))^2 + ((2\zeta r) + r\lambda(1+k^2-r^2)^2} \tag{4.6}$$

Where D is the effective input mass, A is the amplitude of the acceleration, K and M are the sum of the stiffness and mass matrices, ζ is the damping ratio, r is the frequency ratio, λ is the tuning ratio and k is the effective electromechanical coupling.

4.2.5. Experimental performance of a piezoelectric cantilever

Double frequency testing

Since the power profile of a resonance energy harvester has a high sensitivity around the natural frequency, the resolution of the tested frequencies (f_2 in Equation 4.2) is higher around resonance. The frequency spacing is kept above 1 Hz since having a constant frequency less than that is not a focus of this research. Figure 4.8 shows the evaluated frequencies for the piezoelectric cantilever on the frequency response.

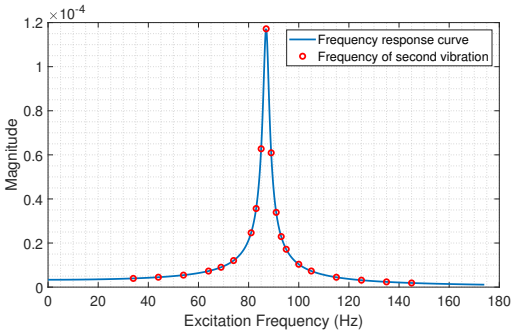


Figure 4.8: Frequency response of the piezoelectric cantilever. The red dots indicate the frequencies that are evaluated during the double-frequency test. Around the resonance peak of the harvester the spacing between the evaluated frequencies is kept smaller.

The instantaneous power P during the experiment is calculated as:

$$P_{load} = \frac{U_{load}^2}{R_{load}} \tag{4.7}$$

Where U is the voltage over the load, and R is the resistance of the load.

Run theoretical model for testing inputs

After the experimental test, the model is ran for the exact excitation settings of the experiment. The inputs for the model (frequency and amplitude) are determined using the following procedure:

1. Identify the beginning and starting point of the 8 seconds segments in the measurement and log the power output. The average power is calculated of the entire 8 seconds so that multiple beating periods are captured.
2. Calculate the STFT of the vibration.

3. Find the amplitudes of the dominant frequencies (A_1 and A_2) per measurement.
4. Calculate the total theoretical power output by summing the powers of both frequencies, using Equation 4.8.

$$P_{theoretical}(f_{normalized}, amplitude) = P_{theoretical}(f_1, A1) + P_{theoretical}(f_2, A2) \quad (4.8)$$

Lastly, the theoretical peak power that is calculated using the model is converted to average power, so that it can be compared with the average power during the experiment. Since the instantaneous power is described by the square of a sine, the average power over one period is half of the peak power amplitude, which can be seen from the following equation:

$$P_{avg} = \frac{1}{T}\int_0^T A \cdot \sin^2(2\pi f t)dt = \frac{1}{2}A \quad (4.9)$$

where A is the peak amplitude of the instantaneous power. An overview of all steps taken to run the theoretical model for the testing inputs is put in Figure 4.9.

4.2.6. Numerical model of a bistable energy harvester

The dynamics of the bistable energy harvester are modelled using Equation 4.10. proposed by Daqaq et al [8]. The model consists of a mechanical oscillator, that is coupled to an electrical (capacitive) circuit.

$$\begin{aligned} m\ddot{x} + c\dot{x} + \frac{dU(x)}{dx} + \theta y &= -m\ddot{x}_b \\ C_p\dot{y} + \frac{y}{R} &= \theta\dot{x} \end{aligned} \quad (4.10)$$

$U(x)$ is the potential function, θ is the electromechanical coupling coefficient, $\ddot{x}_b$ is the base acceleration, C_p is the capacitance of the harvester, y is the voltage and R is the load resistance. The equations are solved numerically in Matlab using an ODE solver.
The instantaneous total power from the simulation is calculated as:

$$P(t) = \frac{(y(t))^2}{R_{load}} \quad (4.11)$$

Since the coefficient θ is fitted for the whole system, no distinction is made between the two buzzers that are physically and electrically separated.

4.2.7. Experimental performance of a bistable energy harvester

The bistable energy harvester is most efficient at 23 Hz at 1G. Therefore, this frequency and amplitude will form the fixed part of the test vibration. The off-resonance vibration is again varied in both frequency and amplitude. The lowest frequency that can be tested on the shaker is limited by the natural frequency of the shaker and the maximum allowed displacement, and it is 13 Hz. The highest frequency that is tested is 30 Hz, since frequencies above this do not harvest any substantial power.
The instantaneous power during the experiment is calculated as:

$$P_{total} = P_{buzzer1} + P_{buzzer2} = \frac{U_{load1}^2}{R_{load}} + \frac{U_{load2}^2}{R_{load}} \quad (4.12)$$

Run simulation for testing inputs
After the experimental test, the model is run for the exact excitation settings of the experiment. The numerical simulation is repeated for every combination of tested amplitude ratio and frequency. The instantaneous power from the simulation is averaged to calculate the average power for each simulation.

4.3. Results

4.3.1. Linear piezoelectric cantilever

The plots in Figure 4.10 show the summation of the peak power for the measured and simulated power (Equation 4.8). All ratios show that there is a vertical offset between the experimental and analytical power. This offset remains constant for different accelerations. Apart from the offset, it can be seen that the analytic power profile follows the same trend as the experimental one, except for one large peak at resonance.

4.3.2. Bistable piezoelectric harvester

The fixed frequency during the double frequency test was meant to be 23 Hz at 1G, however, due to limitations in the maximum displacement of the shaker a maximum amplitude of 0.9 G could be achieved. With this fixed vibration, the second frequency varies from 13 to 30 Hz, with a resolution of 1 Hz. Each frequency is held constant for 10 seconds.
Experimental power - Figure 4.11 shows the average power per frequency for all tested ratios. Also, low and high-energy orbits are indicated, which represent the upper and lower boundaries on the power at 23 Hz, which were found during the frequency up- and down sweeps. These boundaries

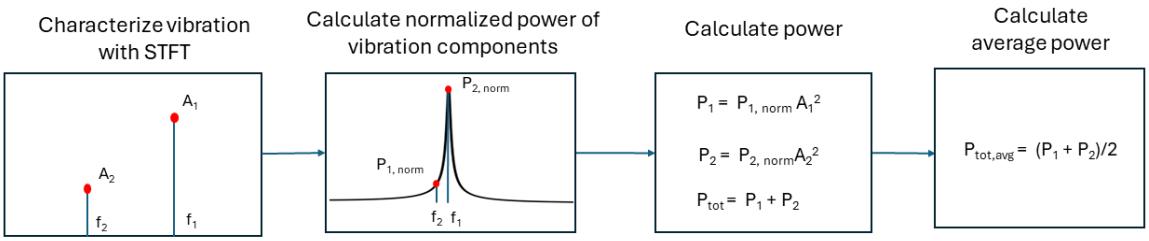


Figure 4.9: Steps taken to calculate the theoretical expected power, for the double vibration used during the tests.

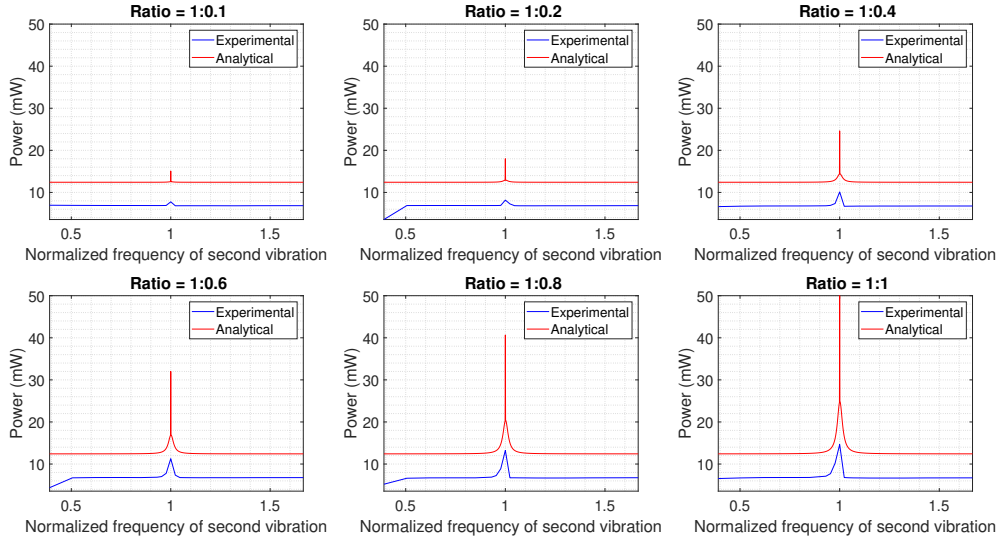


Figure 4.10: Average power for the double frequency experiment of the piezoelectric cantilever. The plot shows the measured average power and the predicted power using the model. The amplitude ratio (A2/A1) is stated in each subplot.

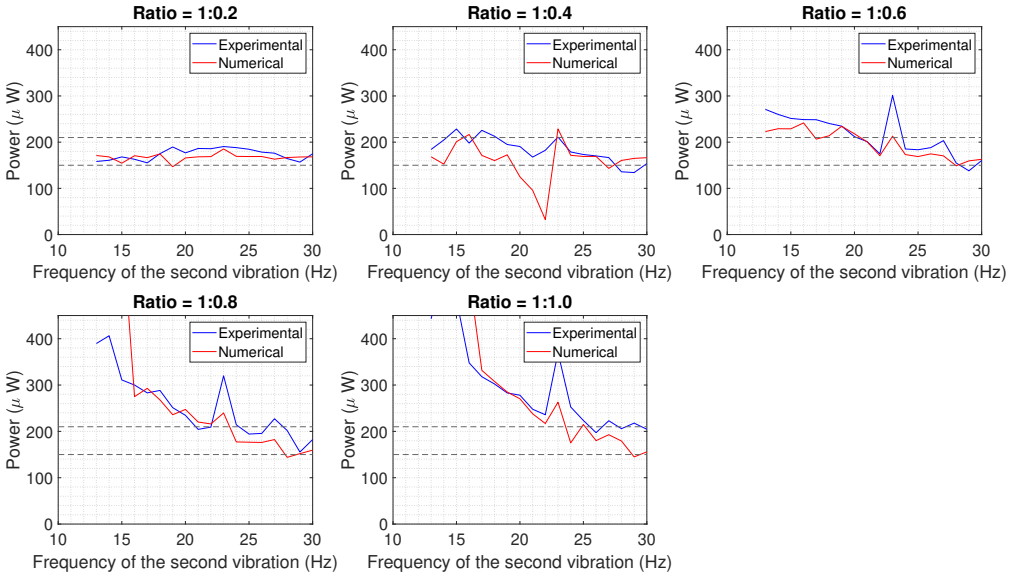


Figure 4.11: Average power during the double frequency tests. Fixed frequency is 23 Hz and 0.9G, the second frequency varies from 13 to 30 Hz. The different amplitudes of the second frequency can be found in the titles. The dotted-horizontal lines indicate the low- and high-energy orbits of the harvester that were found during the frequency sweep. The amplitude ratio (A2/A1) is stated in each subplot.

therefore indicate the expected power of the fixed component of the vibration and variation. For a ratio of 1:0.2 the double vibration seems to have a small effect on power output since the power stays between the low and high energy orbit over the whole frequency range. Close to 23 Hz the average power lies between the low and high energy orbit, whereas for frequencies further from 23 Hz the average power output seems to approach the low energy orbit.
For ratios higher than 1:0.2, the power input generally increases. Only for frequencies above 27 Hz (ratio 1:0.4 and 1:0.6), the double vibration seems to have a negative influence: the output power falls below the low-energy orbit and thus the second component of the vibration has a negative effect on the power output.
When the second vibration is 23 Hz, the two vibrations have the same frequency. Thus the tested signal is a single sine with amplitude $A_1 + A_2$. A clear peak at this frequency is seen in the plot. Also, it is interesting to point out the scaling of power when the second frequency lies within the bandwidth: it can be seen that there is only a minor increase in power for frequencies within the bandwidth of the harvester while the two excitation frequencies are different.
Theoretical power - Figure 4.11 shows a similar trend for the power calculated with the numerical simulation: the powers increase for higher acceleration levels, where the low-frequency accelerations contribute the most to the total output power. The powers of the tested ratio 1:0.4 show a few outliers, where the output power drops by a factor of ≈ 7 at 23 Hz compared to the ratio of 1:0.2. This is counterintuitive since more kinetic input energy is translated into less power. This decrease in power was not seen during the experiment.
The peaks in power that were seen at 23 Hz during the experiment also show in the simulated results. However, the peaks are relatively lower than those from the experiment.

4.4. Discussion

4.4.1. Linear design

Linearity of the linear energy harvester

From the theoretical model the output power of the harvester is expected to scale with the $amplitude^2$ (see Equation 4.6). The experiments show that the power indeed increases around resonance, but that there is a mismatch between the experimental and analytical power profiles. Figure 4.12 shows the scaling of power for an increasing amplitude at 87 Hz. It can be seen that because of the mismatch in eigenfrquency, the power increase is less than $amplitude^2$. This mismatch is a result of unmodelled nonlinearities. By doing multiple frequency sweeps at different excitation amplitudes, it can be seen that the linear cantilever shows a nonlinearity, where the resonance peak shifts to lower frequencies for higher acceleration levels (see Figure 4.13). However, *if* accounted for the the shift in eigenfrequency, the power scales quadratically.

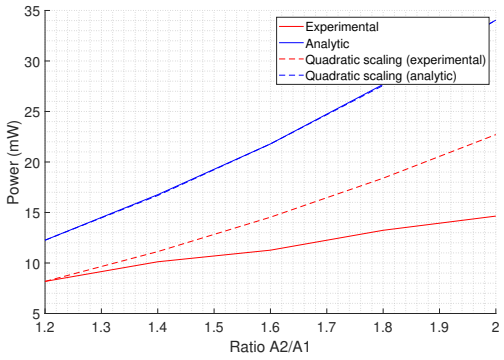


Figure 4.12: Comparison of how the output power scales for an increasing amplitude (at resonance). Solid lines show the real experimental/analytic powers, and dotted lines show the quadratically extrapolated powers to check if the output indeed does scale quadratically in pratice.

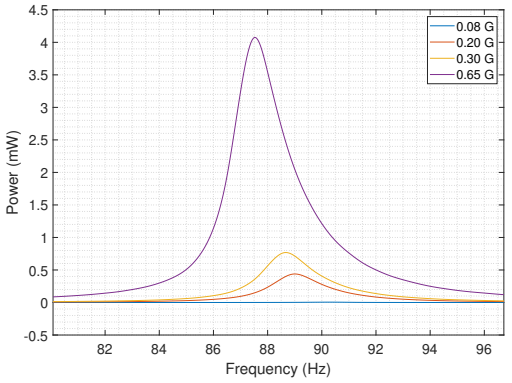


Figure 4.13: Experimental power profiles for different frequency sweeps with different. Note how the resonance frequency shifts downwards for higher accelerations.

During the experiment the amplitude is increased systematically, with that the eigenfrequency is also shifted, which causes the steady state frequency of 87 Hz to not coincide with the eigenfrequency, which subsequently lowers the output power of the theoretical model. For practical applications it is therefore important to define the eigenfrequency of an energy harvester at the amplitude that is representative for a certain environment.

4.4.2. Bistable design

Scaling of power

For linear energy harvesters, the output power theoretically scales with the input $amplitude^2$. The double vibration tests showed that this is not the case for the bistable energy harvester. This is likely the effect of the variation in stiffness.

The stiffness of a linear harvester is constant and thus the force increases linearly with deflection. But the bistable energy harvester has a stiffness that is at least cubic. Therefore, it costs more energy to convert the input acceleration to deflection of the piezoelectric material for higher deflections of the nonlinear spring. This should therefore be taken into account when selecting an energy harvester for environments that show large variations in acceleration amplitude. For example, by using multiple linear harvesters or decreasing the nonlinearity to lower this effect.

Figure 4.14 shows the scaling of output for an increase in amplitude. It can be seen that both colors scale approximately linear. However, both the experimental and simulated powers show a sudden jump in output power. For the experiment, this jump was positive, and for the simulation, it was negative. After inspecting the phase portraits, the simulated data showed that the negative jump was a result of the harvester moving around one stable point.

The main conclusions that can be drawn from this are 1) that the power output scales approximately linear for a nonlinear harvester with an increasing amplitude, and 2) that due to the nonlinearity simulation alone can result in wrong conclusions.

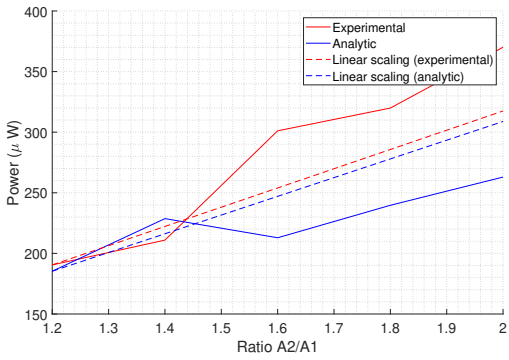


Figure 4.14: Comparison of how the output power scales for an increasing amplitude (at 23 Hz). Solid lines show the real experimental/simulated powers and dotted lines show the linearly extrapolated powers to check the correspondence with linear scaling.

Attribution of low-frequency vibrations to power output

By increasing the amplitude of the vibration, it was shown in Figure 4.11 that the power scales around resonance (which was seen for the linear harvesters as well) but also that the harvested power increases for low frequencies. From this, it can be concluded that by increasing the amplitude a second regime emerges where power can be harvested.

This was shown experimentally and numerically, which proves that the simulation can capture this effect and thus, a device can also be optimized for it.

Comparison between single and multi sine harvested power

During the double sine test, there is one point where both frequencies align, and thus there is only one effective frequency acting on the harvester. For the bistable energy harvester this point lies at 23 Hz.

Figure 4.11 shows that at this frequency there is clear peak in output power. For resonance-based harvester this is explainable because of the limited bandwidth, but for the nonlinear harvester this was not expected. Even when one frequency is 22 Hz, and the other 23 Hz, both frequencies lie within the bandwidth that was found during the single-sine frequency sweep. One would therefore expect that the harvested power would be similar for this case, as the power for a single sine with double the amplitude.

This result shows the limitation of the single frequency sweep, which is that the effective bandwidth for the second frequency is much smaller, meaning that it contributes less to the total power when two harmonic frequencies act on the energy harvester at the same time.

Hysteresis in experimental results

During the double sine experiments, the frequency is increased step by step. Thus, each measurement is followed directly by another. This causes each test to have slightly different beginning conditions (in terms of position, speed, and acceleration). Since a nonlinear systems its behavior is dependent on its history, this could have an effect on the measured power output. One way this might have influenced the results is that the system could sustain its high-energy orbit because of its initial velocity, whereas it would not have been able to reach its high-energy orbit if the system had been excited from a standstill.

In the simulation, each measurement is started from a standstill. Therefore this causes a discrepancy between the experiment and simulation. Also, it might explain why the scaling of power at 23

Hz is more pronounced in the experiment than in the simulation: the system contained more energy at the start of the measurement, and this made it easier to reach a high-energy orbit.
This could have been prevented by starting each measurement from standstill, that way the conditions for the experiment and simulation are the same.

4.5. Conclusions

In this research, a linear and nonlinear piezoelectric energy harvester were tested and modeled for double dominant vibrations.
For a linear harvester it was shown that a model can overpredict the power output due to parasitic nonlinearities, but the experiments and tests also showed that the absolute magnitude of the power profile can be predicted well for double harmonic frequencies. Thus the model is able to accurately predict output power for low excitations, if accounted for a shift in eigenfrequency. This implies that the model can be used to optimize a cantilever for a specific multi-frequency excitation signal.

For a bistable harvester it was shown that a lumped parameter numerical model can predict power output for a double dominant vibration. The results showed that for a single-frequency vibration, the power scales approximately linear with amplitude compared to (almost) quadratic scaling for the linear harvester. This could, therefore, be a motivation to select a linear harvester over a nonlinear vibration for environments with high constant harmonic accelerations.
Also, it was shown that the interference between the double-dominant vibrations has a detrimental effect on the scaling of output power; even for frequencies within the bandwidth of the harvester, a second frequency has a low attribution to the total power (Figure 4.11). Therefore, frequency sweeps can give a false picture of the usable bandwidth of a nonlinear harvester: for a second vibration, there seems to be a small bandwidth in which it can contribute to more output power - just like a linear energy harvester. This presses future research to also test energy harvesters with double frequency sweeps besides standard frequency sweeps, to indicate how well a harvester can absorb multiple harmonic frequencies simultaneously. Lastly, the data clearly showed that bistable energy harvesters work best for low-frequency vibrations. This is a motivation for selecting a nonlinear harvester over a linear one for environments where most energy is contained in the lower frequencies.

5

Reflection, conclusion & recommendations

5.1. Overview of research activities

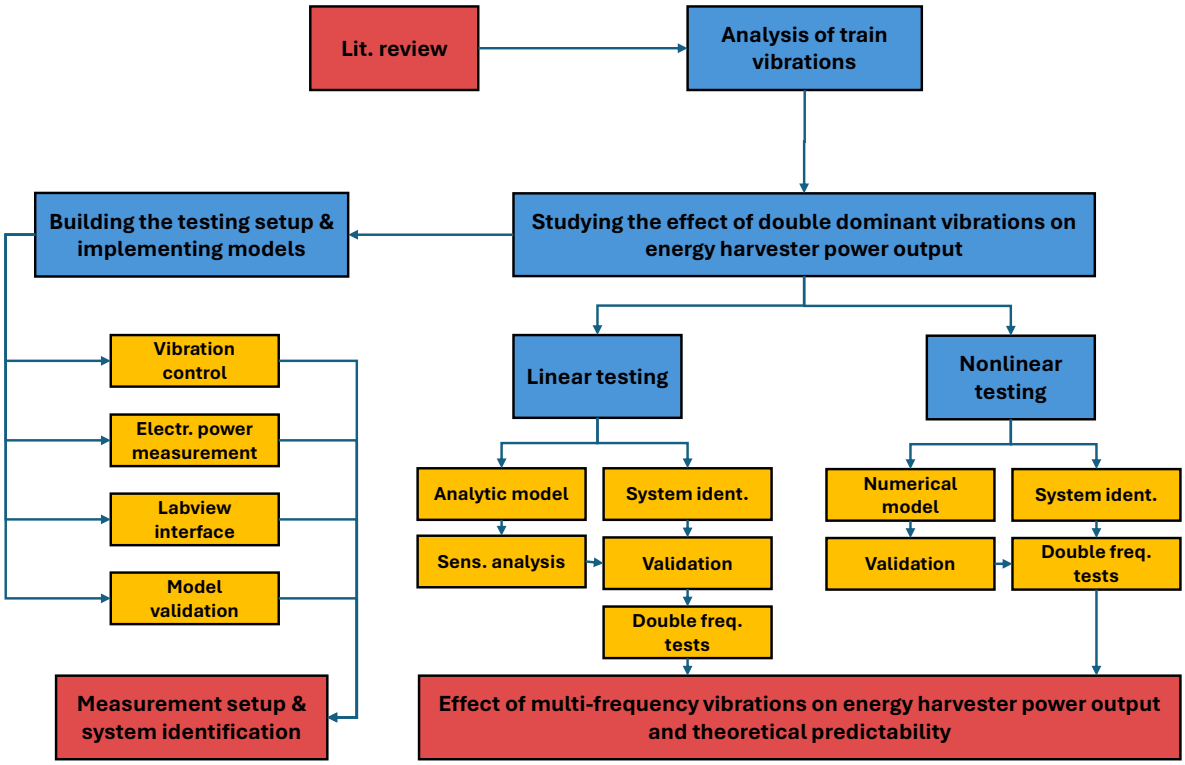


Figure 5.1: Overview of research activities during thesis. Red indicates a paper, blue indicates the main-phases and yellow indicates activities & achievements.

Figure 5.1 contains an overview of how I spent my 10 months at MEMSYS during the thesis.
The thesis started with a literature review of 3 months. The outcome of the literature review was an overview of methods that can be used to calculate the expected power output of linear and nonlinear energy harvesters. After analyzing accelerometer data from trains, it was found that when the train is driving at a constant speed, there are a few frequencies that contain a large amount of the total vibration power (explaining the term 'dominant vibrations'). However, the overview that was made

in the literature review did not contain methods to predict power output for these types of signals. Therefore, this gap became the focus of my research.
The first challenge was creating, and mostly figuring out, how to test the energy harvesters experimentally. Step-by-step a testing setup was built that could be used to measure the power output of energy harvesters, with a controlled vibration level and live power and acceleration output. Then, the setup was used to test a linear and nonlinear energy harvester for both single and multi-sine vibrations. The third step was implementing models from literature, and calculating the power outputs with these models to see how they would compare the experimental tests. Together, this led to the paper of my thesis 'Effect of multi-frequency vibrations on energy harvester power output an theoretical predictability'.

5.1.1. Successes

- 2 models were successfully implemented and tested for energy harvesters that are used within MEMSYS. Both models model the coupling between the mechanical and electrical domain and are therefore more accurate than simpler velocity-dependent models. I hope these models will form a basis for further research within the company.
- A basic test setup was created with (relatively) simple equipment that is easy to use. Also, with the setup impedance matching could be done in a few minutes instead of multiple hours.
- I started my thesis with almost no knowledge on building circuits and taking measurements. Throughout the thesis I learned how to design, build and select components for an experiment.
- By testing energy harvester with double frequencies, the limitations of single sweeps were discovered, which can help future research by using multi-frequency frequency sweeps as an extra performance metric and it creates awareness of how to interpret the frequency response data for a bistable nonlinear harvester.

5.1.2. Unsuccesful attempts

- The original goal of the thesis was to study the effect of multiple dominant frequencies that were surrounded by noise. However, making a control system with feedback was not possible with the equipment that was available at that time. Therefore, an open-loop system was made. Although this approach made it possible to produce constant acceleration sines, it did not work for producing white noise. The problem lay in unwanted excitation of the eigenmode of the shaker, resulting in non-white noise with a peak at the natural frequency of the shaker. Therefore, this part was excluded from the research.
- The model used for the piezoelectric cantilever was made for a fully covered bimorph. The test object, however, was a partially covered unimorph. With a mode shape analysis for the test object, it should have been possible to adjust the model for this. However, this new mode was harder to implement than expected. Therefore the discrepancy between the model and actual design was eventually solved by introducing a fitting parameter for the piezoelectric coupling coefficient.

5.2. Discussion

This research started with a literature review, in which an overview was made of models that can be used to predict the power output of linear and nonlinear energy harvesters. It was found that a variety of models exist, but that these are made and tested for specific types of idealized vibrations.

Next, train vibrations were analyzed to find what type of idealized vibration matches the vibrations on a train to determine which model can be used to predict the output power of energy harvesters. Here, it was found from practical data that train vibrations have a characteristic pattern that was not tested and validated with the existing models. What is unique about the train vibrations is the continuous rise and fall of the acceleration amplitude due to interference between dominant frequencies.
This gap raised the question of whether existing models can be used to capture the effect of beating on the power output. Also, currently, many design papers use single-sine frequency sweeps as a performance metric of how much energy a harvester will output at certain frequencies; so far, no literature was found on how valid this performance metric is for energy harvesters in a multi-frequency environment.

This research tested a linear and nonlinear energy harvester with a vibration signal containing two

dominant frequencies to imitate the effect of beating. An analytic model for a piezoelectric cantilever was implemented and validated for this type of vibration, and it was concluded that the model can predict energy harvester power output *if* accounted for a shift in eigenfrequency due to unmodelled nonlinearities. Also, a bistable nonlinear harvester was tested and modeled. It was shown that average power can be accurately predicted with a model under multi-frequency excitations. Also, it was found that by increasing the excitation, a second 'resonance' regime emerges at low frequencies that can be used to harvest power. Lastly, the results showed that the bandwidth found using a single frequency sweep is not a good predictor of the bandwidth in which energy from different vibration frequencies can be absorbed simultaneously. The results showed that the bandwidth of the double sine experiment was much smaller than that of the single sine frequency sweep, indicating that the interference decreases the power output in the resonance regime found during the single sine frequency sweep.

Combined, this thesis followed a structured approach of modeling energy harvesters by starting at the origin - analyzing the vibration patterns - and setting up tests that approximated the real-life vibration characteristics found in the analysis of the vibration pattern. It showed how existing knowledge in literature should be extended to more realistic scenarios and exposed the limitations of ordinary frequency sweeps.

5.3. Conclusions

Energy harvesting has a promising future ahead. However, steps need to be made before it can be reliably implemented on a large scale.
This research showed the effect of double harmonic frequencies on energy harvester power output and the ability of models to capture this effect. It was shown that the models tested in this research can provide value in understanding and potentially optimizing energy harvesters, even for double harmonic frequencies. The research showed the limitations of single-frequency sweeps compared to double-frequency sweeps, where the beneficial bandwidth of nonlinear energy harvesters disappeared. Therefore, it is recommended that future research uses multi-sine frequency sweeps for nonlinear harvesters as an extra performance metric to better present real-life energy harvester power output.
However, the current models are far from complete to fully capture the energy harvesters' complexity. First, the models still partially rely on experimental parameters, which limits the ability of optimization across a large set of parameters. Secondly, the models used in this research capture the electromechanical coupling to a certain extent. Both models assume that power can be harvested over a pure resistive load, while in reality there is a more complex energy harvesting circuit connected to the piezo element to store the energy. This assumption reduces the number of freedoms and makes the model easy to understand, but it also creates uncertainty in how the power output changes when connected to an energy harvesting circuit.
When continuing to work on these challenges, energy harvester output will increase, giving rise to a new generation of battery-free sensors.

5.4. Recommendations

5.4.1. General remarks

- When performing measurements, you might be tempted to only look at the final outputs of the test; for example the average output power of an energy harvester. But it is also important to always check all the raw signals that you measured. The raw signals often give you more information about possible errors in the measurement. Some of the issues I've encountered: clipping of voltage signals, DC offsets in AC signals, low signal to noise ratios and wires that were loosening over time due to the vibrations resulting in momentary losses in power.
- The hardest challenge in energy harvesting is the link between a mechanical and electrical system. As a mechanical engineer you understand part of the system, and vice versa for an electrical engineer. Therefore I would really recommend talking to people with electrical background about assumptions you make, things you do & do not understand and the practical implementation of a system. These conversations will confuse you, but also give a lot of food for thought and, in the end, will give you new ideas.
- If possible, do all tests in one go. You will notice that prototype energy harvesters will deform

over time and their properties will change. By doing all tests after each other, it is easier to lay the link between different results and it will decrease the possibility of false-conclusions.

5.4.2. Futher research directions

- **Investigate scaling of damping for piezoelectric cantilevers**
  The model used for the piezoelectric cantilever in this paper used Rayleigh damping to determine the damping ratio of the system. Getting accurate damping coefficients with this method is hard. When using the model to optimize a design, this causes big uncertainty since the power output is roughly dependent on the ratio between electrical and mechanical damping. In an optimization problem, this becomes problematic because you cannot measure the added performance of a larger/thicker piezoelectric patch since its effect on mechanical damping is unknown. By doing more experiments, one could get a better idea of how the damping changes for a change in design parameters. It would already be helpful to fix the length and width of a cantilever, and vary the surface area covered by piezoelectric material and measure the mechanical damping ratio for each case.
- **Piezoelectric coupling coefficient**
  After producing the bistable mechanism, the piezoelectric coupling coefficient was measured experimentally. Similarly to the above point, this creates a gap between modeling the performance of a design and knowing the effect of its input parameters. Since the power output of a piezoelectric element is dependent on the deformation/stress in the piezo, a study could be performed on how this coefficient is coupled to its design parameters. This could be done by focusing on one type of design and systematically changing the surface area, thickness, or placement of the piezo element to study the effect on power output. By modeling the effect of the design changes in Comsol it should hopefully be possible to find a relation between the piezoelectric coupling coefficient, and the ratio between (for example) the elastic energy in the piezo element and the whole system.
- **Parametrize force deflection curves**
  The force-deflection curve greatly affects the dynamics of a nonlinear energy harvester. Let's say you are trying to find the theoretical most optimal force-deflection curve for a certain vibration; then the next step is to actually produce it. By creating an overview of how certain parameters affect the force-deflection curve (pre-tension, width, length etc.), you could create a database that can be used to tweak designs to match the wanted force-deflection profile. Also, it will give insight into how sensitive certain parameters are, which will be very valuable for (mass)production. This information could eventually be used to decide what production process is needed to meet the precision needed for a reliable design. Here, the biggest challenge lies in creating a test setup with high precision.
- **Find out if you can reach a minimum power output by increasing the size of a harvester systematically**
  Many design papers try to optimize and test a prototype to eventually come to the conclusion that their harvester can not be applied (yet) to a real-life application because of too low power output. Although this limitation is an interaction between harvesting more power and consuming less energy, I would say it is interesting to set a goal of how much power a design needs to harvest and iterate towards a design that meets this power output by increasing its size. The motivation for this is that it becomes easier to harvest more energy when you have more mass and design space. Some environments require small designs, but industrial applications might not always care about size (to some extent). Therefore this would be a relatively easy way of upsizing existing design to show and prove the future of energy harvesting, and maybe already apply it soon.
- **Implement boundary conditions in models**
  Currently, the models used in this research do not consider boundary conditions such as maximum yield stress within the piezoelectric material, or maximum allowed absolute deflection. This needs to be implemented if someone wants to use the model to optimize designs. Without these boundary conditions, it will yield unreliable and unfeasible designs.

Acknowledgements

First I would like to thank my supervisors Thijs Blad and Gerard Verbiest. Working under their guidance has been really learnful and enjoyable, which made the past 10 months fly by. Thijs has always been really approachable and helped whenever asking for it. I also much appreciated the biweekly meetings with Gerard, where he often came up with ideas that I, or people from MEMSYS, did not think of. Together, they learned me how to set up a research, do measurements and be critical.

I also would like to thank all people from MEMSYS, especially Dion Hogervorst & the interns. Dion was always in for a talk about the project and other stuff. These talks often led to hypotheses about the problems I had throughout my research.
The group of interns made the year memorable. The countless games of pool, Friday drinks, made-up sayings and discussions about Drievliet (amusement park in Rijswijk) kept me motivated throughout the year.

Lastly, I would like to thank my family and friends. Not only did they show interest in my project, but they also brought lots of fun, love, and support, which helped me to relax from the project whenever needed.

Thanks.

References

[1] E. L. Pradeesh et al. "A review on piezoelectric energy harvesting". In: *Microsystem Technologies* 28.8 (June 2022), pp. 1797–1830. ISSN: 1432-1858. DOI: 10.1007/s00542-022-05334-4. URL: http://dx.doi.org/10.1007/s00542-022-05334-4.

[2] EnABLES Consortium. *EnABLES Research Infrastructure Position Paper*. https://www.enables-project.eu/wp-content/uploads/2021/02/EnABLES_ResearchInfrastructure_PositionPaper.pdf. Accessed: 2024-09-16. 2021.

[3] Imededdin Djadour, Salih Aidel, and Hicham Medkour. "Design and implementation of low power consumption wireless sensor node". In: 17 (Sept. 2019), pp. 2729–2734. DOI: 10.12928/telkomnika.v17i6.

[4] Victoria J. Hodge et al. "Wireless sensor networks for condition monitoring in the railway industry: A survey". In: *IEEE Transactions on Intelligent Transportation Systems* 16 (3 June 2015), pp. 1088–1106. ISSN: 15249050. DOI: 10.1109/TITS.2014.2366512.

[5] Shi Yi et al. "On Renewable Sensor Networks with Wireless Energy Transfer". In: IEEE, 2012. ISBN: 9781424499212. DOI: 10.1109/INFOCOM17876.2011.

[6] Tyndall Mike Hayes. *78 million batteries will be dumped every day by 2025*. 2023.

[7] Alperen Toprak and Onur Tigli. *Piezoelectric energy harvesting: State-of-the-art and challenges*. Sept. 2014. DOI: 10.1063/1.4896166.

[8] Mohammed F. Daqaq et al. *On the role of nonlinearities in vibratory energy harvesting: A critical review and discussion*. 2014. DOI: 10.1115/1.4026278.

[9] Robert Rantz and Shad Roundy. "Characterization of real-world vibration sources with a view toward optimal energy harvesting architectures". In: vol. 9801. SPIE, Apr. 2016, 98010P. ISBN: 9781510600423. DOI: 10.1117/12.2219416.

[10] Xiang Wang et al. "A frequency and bandwidth tunable piezoelectric vibration energy harvester using multiple nonlinear techniques". In: *Applied Energy* 190 (2017), pp. 368–375. ISSN: 03062619. DOI: 10.1016/j.apenergy.2016.12.168.

[11] Fglynne-Jones, S P Beeby, and N M White. *Towards a piezoelectric vibration-powered microgenerator*. 2001.

[12] N. G. Stephen. "On energy harvesting from ambient vibration". In: *Journal of Sound and Vibration* 293 (1-2 May 2006), pp. 409–425. ISSN: 10958568. DOI: 10.1016/j.jsv.2005.10.003.

[13] R. L. Harne and K. W. Wang. *A review of the recent research on vibration energy harvesting via bistable systems*. Feb. 2013. DOI: 10.1088/0964-1726/22/2/023001.

[14] Mohammed F. Daqaq. "Transduction of a bistable inductive generator driven by white and exponentially correlated Gaussian noise". In: *Journal of Sound and Vibration* 330 (11 May 2011), pp. 2554–2564. ISSN: 0022460X. DOI: 10.1016/j.jsv.2010.12.005.

[15] Heonjun Yoon et al. "Time-varying output performances of piezoelectric vibration energy harvesting under nonstationary random vibrations". In: *Smart Materials and Structures* 27 (1 Jan. 2018). ISSN: 1361665X. DOI: 10.1088/1361-665X/aa95ed.

[16] Jens Trampe. Broch and Joëlle. Courrech. *Mechanical vibration and shock measurements*. Brüel & Kjaer, 1980, p. 370. ISBN: 8787355345.

[17] Joeri Roos. *Correct examination of vibration energy harvester performance*.

[18] Ali Nayfeh and Dean Mook. *Nonlinear ocillators*. Wiley, 1995.

[19] Chunlin Zhang et al. "Harmonic analysis and experimental validation of bistable vibration energy harvesters interfaced with rectifying electrical circuits". In: *Communications in Nonlinear Science and Numerical Simulation* 82 (Mar. 2020). ISSN: 10075704. DOI: 10.1016/j.cnsns.2019.105069.

[20] Heonjun Yoon and Byeng D. Youn. "Stochastic quantification of the electric power generated by a piezoelectric energy harvester using a time-frequency analysis under non-stationary random vibrations". In: *Smart Materials and Structures* 23 (4 2014). ISSN: 1361665X. DOI: 10.1088/0964-1726/23/4/045035.

[21] A. Erturk and D. J. Inman. "An experimentally validated bimorph cantilever model for piezoelectric energy harvesting from base excitations". In: *Smart Materials and Structures* 18 (2 2009). ISSN: 1361665X. DOI: 10.1088/0964-1726/18/2/025009.

[22] S. Zhao and A. Erturk. "Electroelastic modeling and experimental validations of piezoelectric energy harvesting from broadband random vibrations of cantilevered bimorphs". In: *Smart Materials and Structures* 22 (1 Jan. 2013). ISSN: 09641726. DOI: 10.1088/0964-1726/22/1/015002.

[23] X. Eguiluz et al. "Maximizing harvested energy for linear vibration-based generators". In: vol. 120. Elsevier Ltd, 2015, pp. 641–644. DOI: 10.1016/j.proeng.2015.08.693.

[24] R. S. Langley. "A general mass law for broadband energy harvesting". In: *Journal of Sound and Vibration* 333 (3 Feb. 2014), pp. 927–936. ISSN: 0022460X. DOI: 10.1016/j.jsv.2013.09.036.

[25] D. H. Hawes and R. S. Langley. "Limits on the power available to harvest from broadband random excitation". In: *Journal of Sound and Vibration* 399 (July 2017), pp. 244–256. ISSN: 10958568. DOI: 10.1016/j.jsv.2017.03.036.

[26] L. Gammaitoni, I. Neri, and H. Vocca. "Nonlinear oscillators for vibration energy harvesting". In: *Applied Physics Letters* 94 (16 2009). ISSN: 00036951. DOI: 10.1063/1.3120279.

[27] Mohammed F. Daqaq. "Response of uni-modal duffing-type harvesters to random forced excitations". In: *Journal of Sound and Vibration* 329 (18 2010), pp. 3621–3631. ISSN: 10958568. DOI: 10.1016/j.jsv.2010.04.002.

[28] Gael Sebald et al. "Simulation of a Duffing oscillator for broadband piezoelectric energy harvesting". In: *Smart Materials and Structures* 20 (7 2011). ISSN: 1361665X. DOI: 10.1088/0964-1726/20/7/075022.

[29] P L Green. *Nonlinear Energy Harvesting in the Faculty of Engineering*. 2012.

[30] F. Cottone, H. Vocca, and L. Gammaitoni. "Nonlinear energy harvesting". In: *Physical Review Letters* 102 (8 Feb. 2009). ISSN: 00319007. DOI: 10.1103/PhysRevLett.102.080601.

[31] Mohammed F. Daqaq. "On intentional introduction of stiffness nonlinearities for energy harvesting under white Gaussian excitations". In: *Nonlinear Dynamics* 69 (3 Aug. 2012), pp. 1063–1079. ISSN: 0924090X. DOI: 10.1007/s11071-012-0327-0.

[32] Einar Halvorsen. "Energy harvesters driven by broadband random vibrations". In: *Journal of Microelectromechanical Systems* 17 (5 2008), pp. 1061–1071. ISSN: 10577157. DOI: 10.1109/JMEMS.2008.928709.

[33] Ravindra Masana and Mohammed F. Daqaq. "Response of duffing-type harvesters to band-limited noise". In: *Journal of Sound and Vibration* 332 (25 Dec. 2013), pp. 6755–6767. ISSN: 0022460X. DOI: 10.1016/j.jsv.2013.07.022.

[34] R. van Schaijk et al. "A MEMS vibration energy harvester for automotive applications". In: vol. 8763. SPIE, May 2013, p. 876305. ISBN: 9780819495600. DOI: 10.1117/12.2016916.

[35] Jalal Khaghanifard, Amir R. Askari, and Mohsen Taghizadeh. "Frequency-Domain Analysis of Shock-Excited Magneto-Electro-Elastic Energy Harvesters with Different Unimorph and Bimorph Configurations". In: *Iranian Journal of Science and Technology - Transactions of Mechanical Engineering* 47 (3 Sept. 2023), pp. 1205–1222. ISSN: 23641835. DOI: 10.1007/s40997-022-00575-0.

[36] M Amin Karami and Daniel J Inman. *CONTROLLED BUCKLING OF PIEZOELECTRIC BEAMS FOR DIRECT ENERGY HARVESTING FROM PASSING VEHICLES*. 2012. URL: http://www.asme.org/about-asme/terms-of-use.

[37] R. L. Harne et al. "An analytical approach for predicting the energy capture and conversion by impulsively-excited bistable vibration energy harvesters". In: *Journal of Sound and Vibration* 373 (July 2016), pp. 205–222. ISSN: 10958568. DOI: 10.1016/j.jsv.2016.03.012.

[38] H. A. Sodano, G. Park, and D. J. Inman. "Estimation of electric charge output for piezoelectric energy harvesting". In: *Strain* 40 (2 May 2004), pp. 49–58. ISSN: 00392103. DOI: 10.1111/j.1475-1305.2004.00120.x.

[39] K. Ogata. *Modern Control Engineering*. Prentice Hall, 2010.

[40] Yabin Liao and Henry A. Sodano. "Model of a single mode energy harvester and properties for optimal power generation". In: *Smart Materials and Structures* 17 (6 Dec. 2008). ISSN: 09641726. DOI: 10.1088/0964-1726/17/6/065026.

[41] JPE. *Precision Point 4th edition*. JPE, 2018.

A

Literature review

A.1. Literature review overview

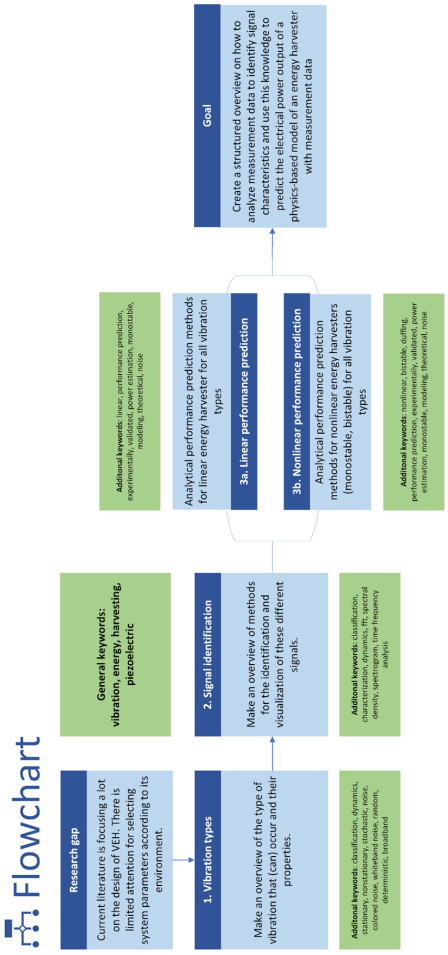


Figure A.1: Visualization of literature review structure an keywords used.

A.2. Signal overview

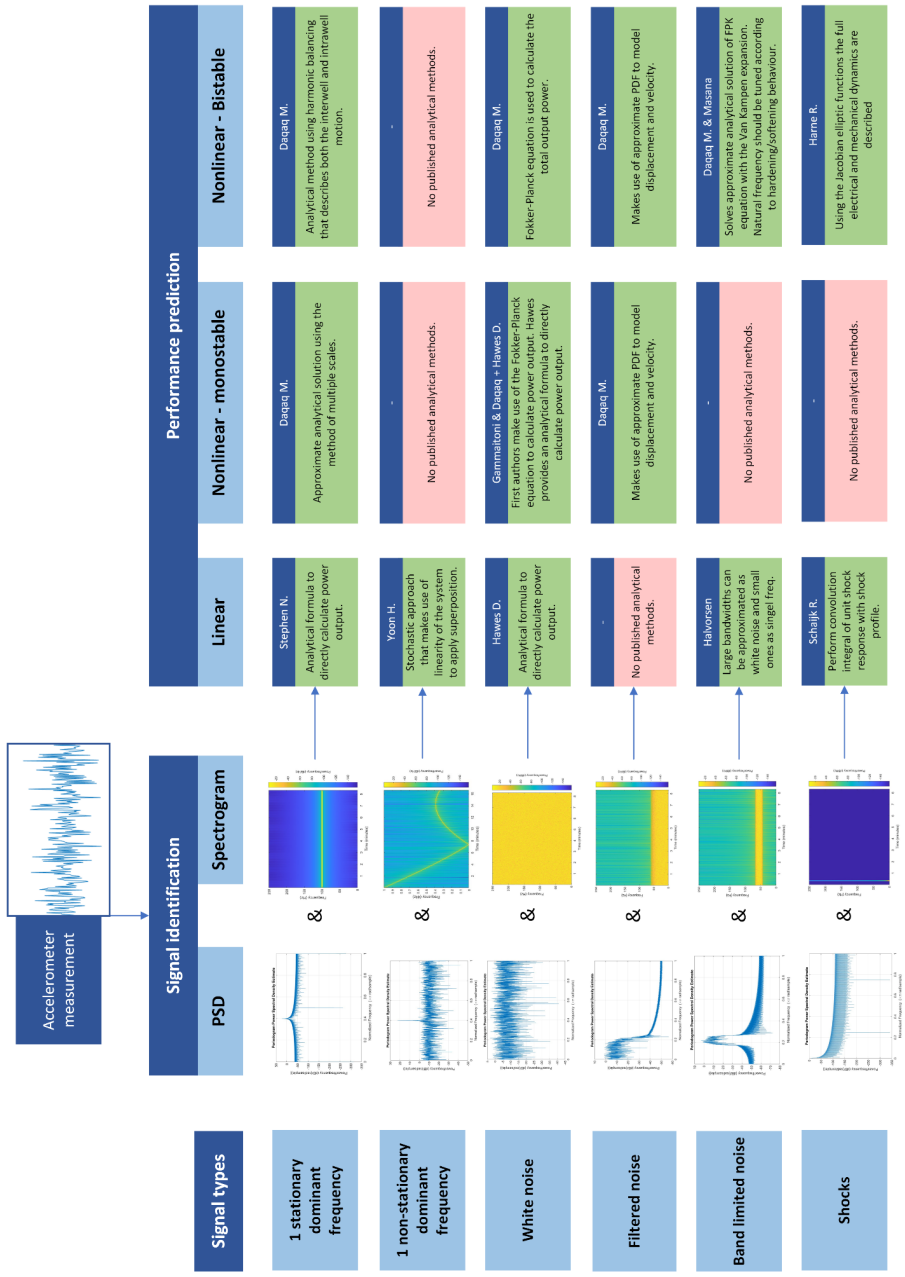


Figure A.2: Overview of found methods in literature that can be used for predicting the power output of energy harvesters.

B

Measurement setup & system identification

B.1. Components and specifications

Overview testing setup



Figure B.1: Overview of testing setup with all components

Decade box



Figure B.2: Decade box. In the picture the variable resistance is set to $10000 + 5000 = 15000k\Omega$

.

Shaker



(a) TIRA TV51140

TECHNICAL PARAMETERS Vibration exciter S 51140

Rated peak force Sine$_{pk}$/Random$_{RMS}$	400/311 N
Frequency range	2-6500 Hz
Main resonance frequency	>5500 Hz
Max. displacement Peak-Peak	20 mm
Max. velocity Sine/Random	1.5/1.5 m/s
Max. acceleration Sine/Random	100/50 g
Suspension stiffness	5 N/mm
Effective moving mass	0.4 kg
Max. weight tested[1]	6 kg
Weight	18 kg
Armature diameter	60 mm

1) Testing weight has an impact on the possible maximum displacement

(b) Parameters of the shaker

Figure B.3: TIRA TV51140 and its corresponding parameters

Accelerometer



Figure B.4: PCB35621 accelerometer

Laser displacement sensors

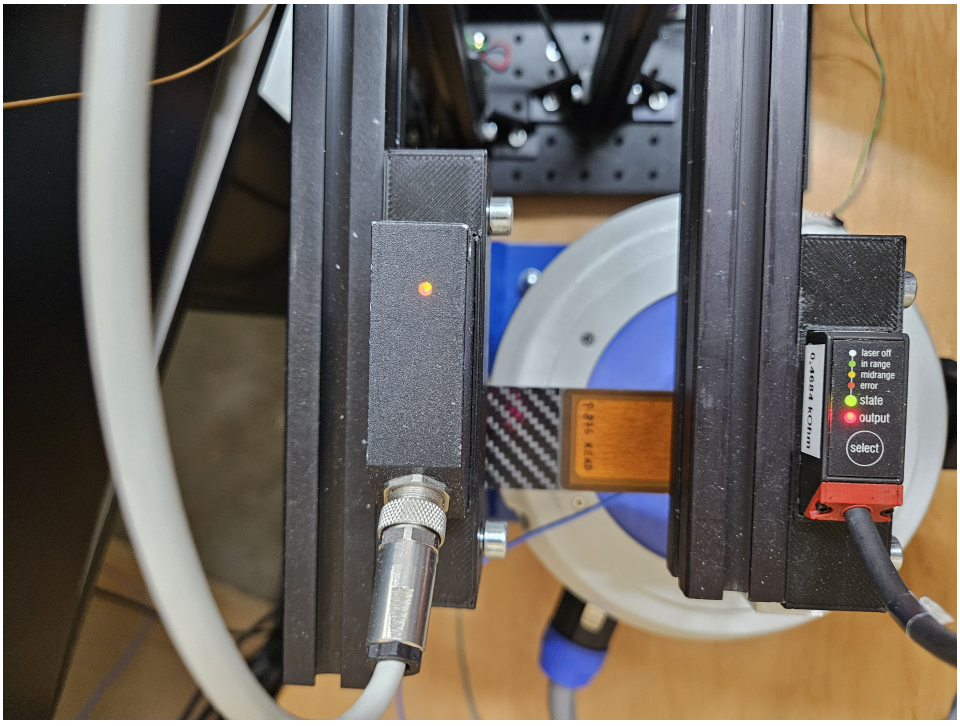


Figure B.5: Laser displacement sensors. Micro-Epsilon NCDT1401 (left) and Micro-Epsilon NCDT1420 (right)

Signal conditioner



Figure B.6: Signal conditioner that supplies the PCB accelerometer with a current. Gain is set to x10 since this gives the highest resolution in the measuring range of the DAQ

DAQ - National Instruments USB-6211

ADC resolution	16 bits
Input range	± 10 V
Input impedance	> 10GΩ
Max sampling rate	250 kS/s

Table B.1: DAQ Parameters

B.2. Labview diagrams

This section contains the Labview diagrams that were used for taking measurements. The *DAQMX configuration* is generic for all models. Its outputs are connected to the diagrams that contain the calculations. Together with the TDMS implementation shown in the diagram, this setup is capable of capturing multiple samples at high sampling rates (tested up to 50000 samples / channel).
It is highly recommended to choose the TDMS file format over .csv or .text. These can store information faster, and are much faster when reading out data in Matlab (minutes vs. seconds!). However, be aware that you properly set up the 'groupnames' of the *TDMS write* block, otherwise Matlab cannot read your data. Also it is smart to always store your calculated values + raw voltages. The voltages can give indication of possible measurement errors, and if you made a mistake in one of your Labview calculations you can correct for it after your measurement since you have the raw data.
Labview - front panel

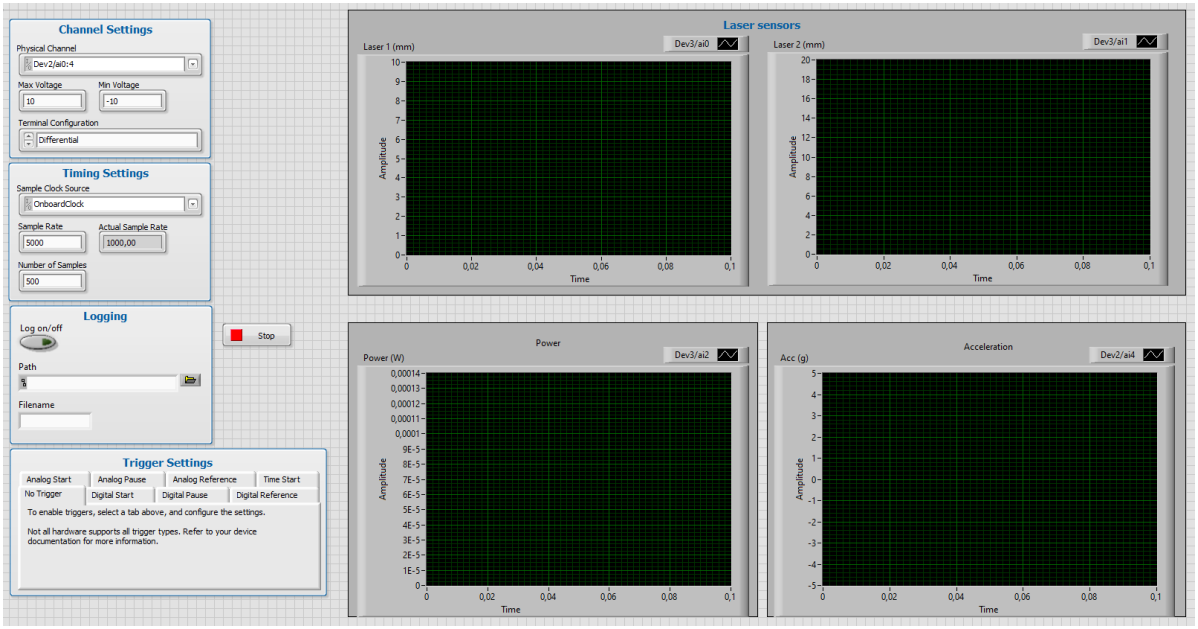


Figure B.7: Labview diagram front panel - snippet 1

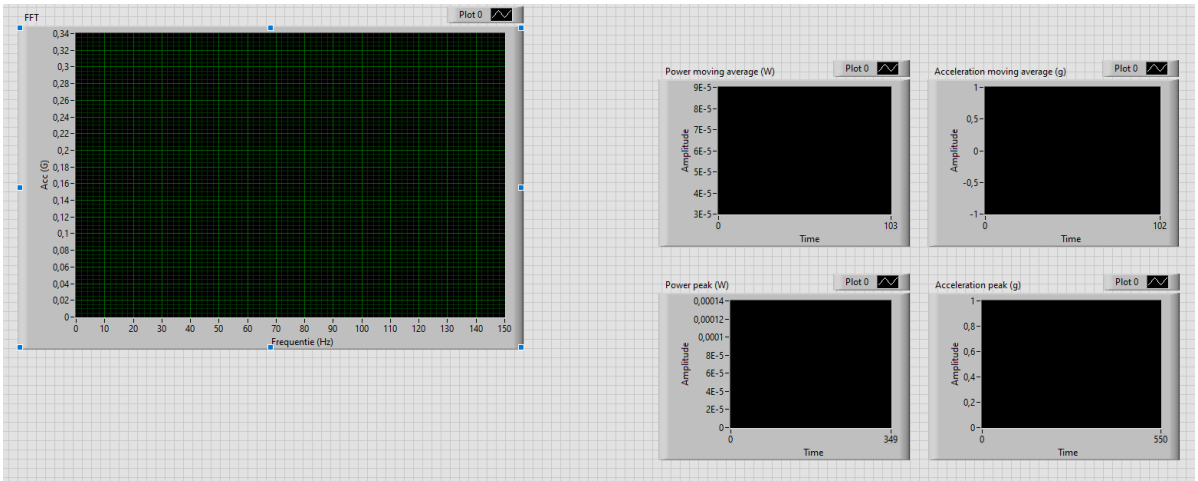


Figure B.8: Labview diagram front panel - snippet 2

Labview diagram - DAQmx configuration

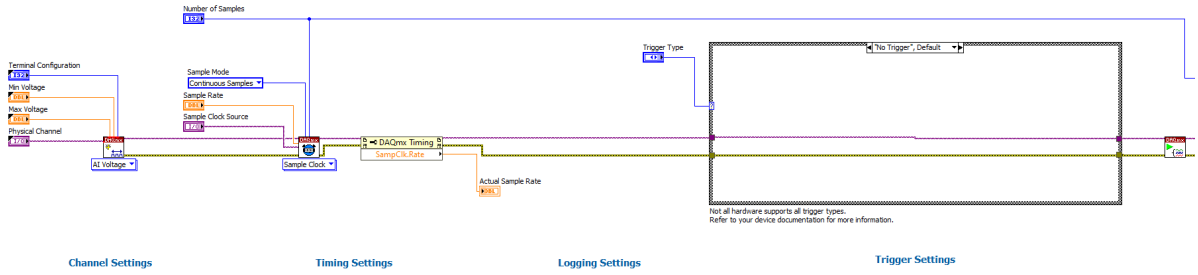


Figure B.9: Labview diagram - snippet 1

Labview diagram - Calculations and visualization used for variable load measurements

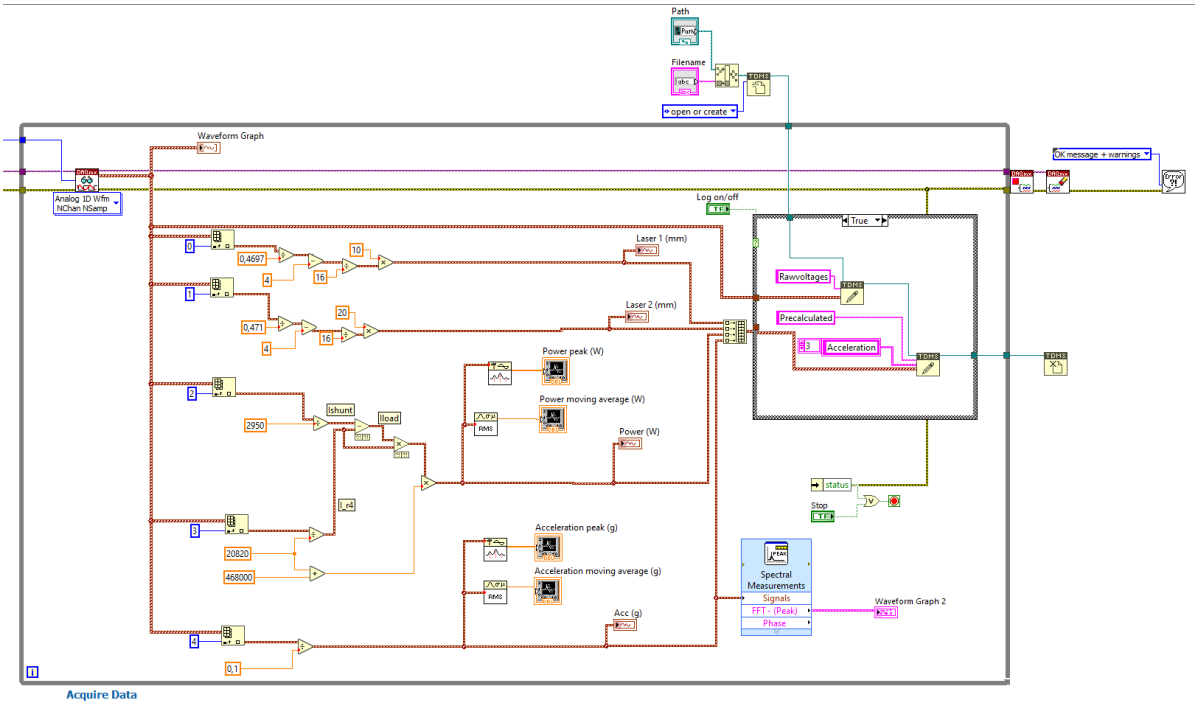


Figure B.10: Labview diagram - variable load measurements

Labview diagram - Calculations and visualization used for fixed load measurements

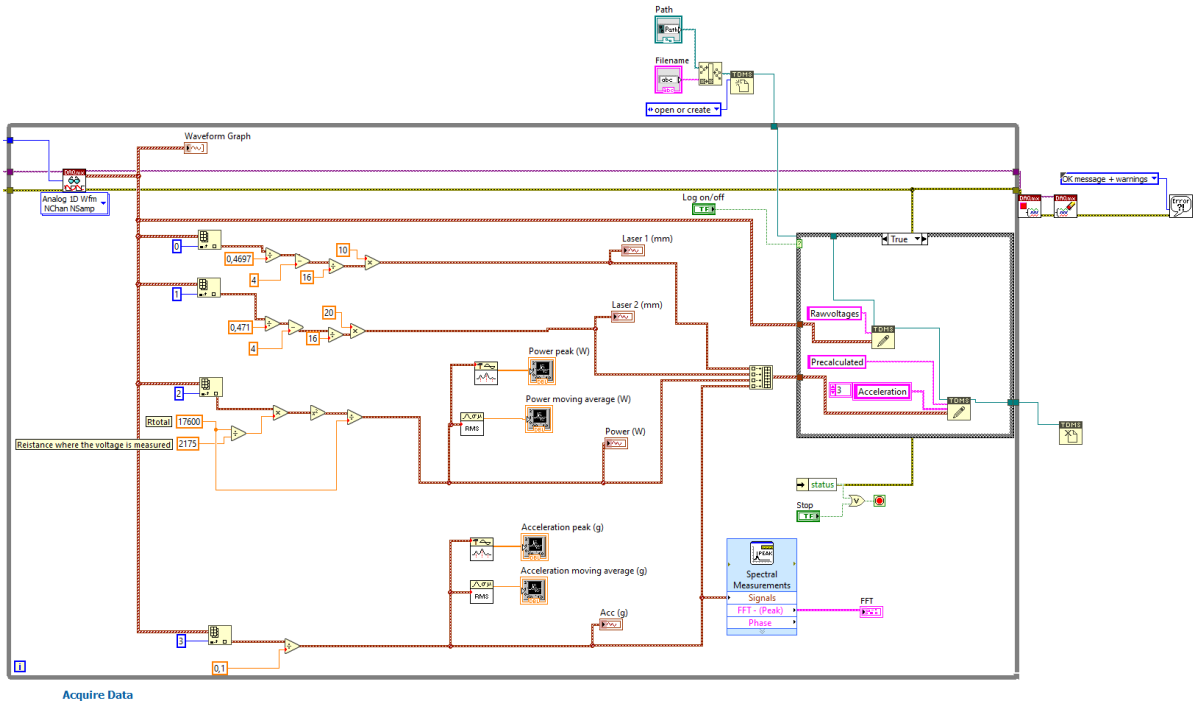


Figure B.11: Labview diagram - fixed load measurements

C

Technical drawings

C.1. PI E-821 Piezoelectric cantilever

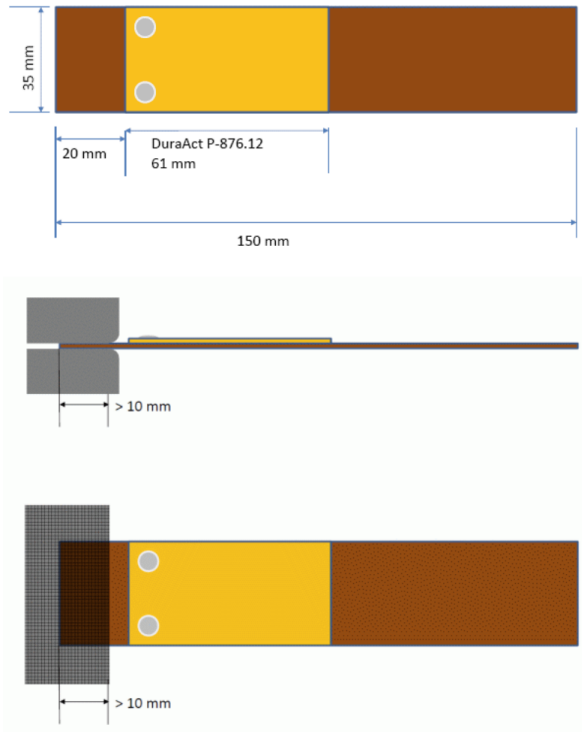


Figure C.1: E-821 Energy harvester from PI Ceramics



Figure C.2: Aluminium clamp used to mount the cantilever to the shaker

D

Sensitivity analysis piezoelectric cantilever

The model that was used to calculate the power output of a piezoelectric cantilever, assumes a fully covered bimorph. Thus, a substrate of which both sides are covered with piezoelectric material.
The test object that was available at that time was a partially covered bimorph. Thus, a substrate of which only one side is partially covered with piezoelectric material.

This discrepancy led to a model which overestimates the power output. Therefore, an adjustment was needed to the model to correctly predict power output for this specific test object. In order to make this adjustment, two things were done. First, a sensitivity analysis was made, to see the effect of the input parameters on estimated power output. This would give an idea of how the uncertainties in input parameters contributed to the overestimated power output. Secondly, a stress calculation was performed to estimate how much power this partially covered cantilever would logically harvest in comparison to a fully covered cantilever.

D.1. Sensitivity analysis

The model used to calculate the power output is based on 14 input parameters, all of which are measured, retrieved from specsheets, or estimated. Therefore, each input has an uncertainty. By doing a sensitivity analysis the error propagation to the total estimated power is calculated for the uncertainty in parameters.

The error propagation vector of the function power function F is defined as:

$$\sigma_F^2 = \sum_i^n \left(\frac{\partial F}{\partial x_i} \right)^2 \sigma_i^2 \tag{D.1}$$

Parameter	Value	Uncertainty (σ_i)	Error propagation (mW)	Error / total power(%)
A	9.81	0.0981	0.105	2
t_s	0.0013	3.9e-05	-0.201	-3.83
t_p	0.0005	5e-06	0.067	1.28
width	0.035	3.85e-05	0.013	0.26
width_p	0.03	3e-05	-0.007	-0.13
L	0.13	3.9e-05	0.005	0.09
rho_s	2000	100	0.094	1.8
c_s	2e10	2e9	-0.032	-0.61
rho_p	7800	390	0.299	5.7
c_p	6.2e10	6.2e9	0.056	1.07
epsilon_s	4.427e-09	4.427e-11	-0.051	-0.96
d_{31}	-1e-11	-1e-13	0.101	1.93

Table D.1: Propagation of error for uncertainty of input parameters and the effect on total power

From Table D.1 it can be seen that the uncertainties in input parameters have a small effect on the total output power. The uncertainty in thickness, resulting from a manual measurement with a caliper, has the largest effect on the total error, which is only a 3.8% error of the total power.

D.2. Decreased power output due to mismatch in model and test object

The overestimation in power is a logical result of a discrepancy between the model and the test object. Since the charge generated by a piezo element is linear with the applied stress, the stress profile over the cantilever beam is analyzed. With that information, an estimation can be made of what percentage of stress in the beam is converted to power, in comparison to a beam of where all stress is translated into charge.

The stress in a cantilever beam as a result of a linear distributed load is defined by [41]:

$$\sigma_x = \frac{qu(L-x)^2}{2I_x} \tag{D.2}$$

Where q is the load, u is the fiber distance, L is the length, x is the coordinate along the length of the beam and I_x is the moment of inertia around the x-axis.
The cantilever beam has a total effective length of 130mm, of which 61mm is covered with piezoelectric material from the base. By integrating the stress with respect to the x-direction, across the whole beam, and across the piezoelectric material, an estimation can be made of the overestimation of the model for this cantilever:

$$\text{Factor of lost power} = \frac{\int_0^{61} \sigma_x(x)dx}{\int_0^{130} \sigma_x(x)dx} = 0.452 \tag{D.3}$$

However, this correction factor does not yet account for the fact that the test object is unimorph. Thus, the final correction factor is halved. This gives a final correction factor of 0.23.

D.3. Conclusion

Initially, the output power of the model was overestimated by a large factor. By doing a sensitivity analysis, it was shown that the uncertainty in some of the parameters did not have a substantial effect on the total error. Next, the mismatch in power between the model and the test object was investigated by analyzing the stress in the beam. From this analysis, a correction factor of 0.23 was found. After applying this factor to the model, it was found that the power profile of the model and experiment perfectly overlapped.

E

Error analysis & improvements

E.1. Validation of true train vibrations

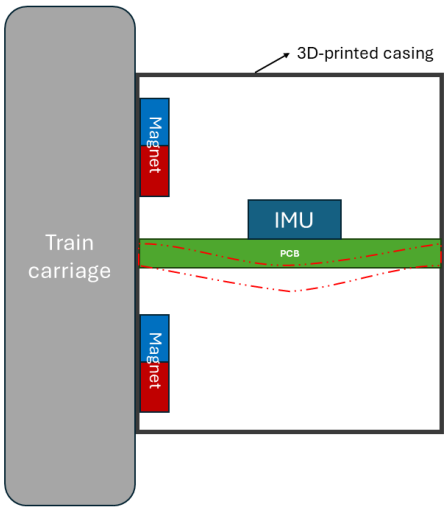


Figure E.1: Sketch of the IMU placement within the sensor. The red-dotted line shows the possible deformed position of the PCB due to the vibrations that could magnify certain frequencies and create 'false' dominant vibrations.

The main research question followed from the analysis of accelerometer data. This data was captured using a custom device. The device consists of a 3D-printed housing, with a commercial printed circuit board (pcb) that contains an accelerometer. The device is mounted on the side of a train with neodymium magnets.
Since the accelerometer is not mounted directly on a stiff part of the train carriage, the measured acceleration could be affected by the eigenmodes of the custom device. For example, the housing or pcb can resonate in its eigenfrequency.
This could mean that the dominant vibrations that were identified only exist on the pcb of the custom sensors, and thus not on the undercarriage of the train; which is the place were an energy harvester would be mounted. In the end, this could have created a false conclusion about the characteristics of vibrations that were found on the train.
The first step in getting more reliable data would be to make a transfer function of the acceleration measured at the base of the casing (close to the magnet) to the acceleration measured with the IMU of the sensor. This would give information about what frequencies are amplified, together this information could then be used to back-calculate the real vibrations of the train from the measured acceleration. Even better would be to do a test with a calibrated accelerometer, that contains an anti-aliasing filter

(which the current sensor did not have). If such a sensor could be mounted directly on the undercarriage of the train, it is most likely that the measured vibrations are the *true* vibrations.

E.2. Unwanted excitation of eigenmode of the shaker

During the experiment a feedforward signal is sent to the shaker. Since there is no feedback control, the snap-through motion of the energy harvester is a shock input to the shaker and therefore activates the eigenmode. Therefore, some 'unwanted' frequencies are being fed from the shock of the energy harvester into the shaker which causes the testing signal of a 'double vibration' to become a double vibration + the vibration of the suspension mode of the shaker. Especially for comparing the simulated and experimental results, this creates an error.
In the end, the error was minimized by adding a mass to the shaker to increase its inertia.

E.3. Inconsistencies in bistable design

The bistable design that was produced and tested in this research consisted of a 3D-printed casing. A 3D-printed casing was chosen because milling was too time consuming. However, this caused three types of error.
Print accuracy - The first type of error is the accuracy of the 3D printer, which causes each print to be slightly different, making it hard to produce similar designs. This caused some prints to be monostable and others to be too bistable. Therefore, the method of using 3D-printed designs is not scalable for mass-production.
Creep - Another problem with using 3D-printed design is creep. The reactive force of the compressed flexure caused the PLA to elongate, making the design to have slightly different characteristics over time. Therefore all tests with the bistable harvester were conducted in one go, making the effect of creep as small as possible. Nevertheless, PLA is not a durable solution for an energy harvester that will be used in the field since a slight amount of creep can change the characteristics drastically.
Slip - The flexure is clamped on both ends with 3D-printed brackets. These brackets are tightened as strongly as possible; however, sometimes, it seems that the flexure slipped within the bracket.

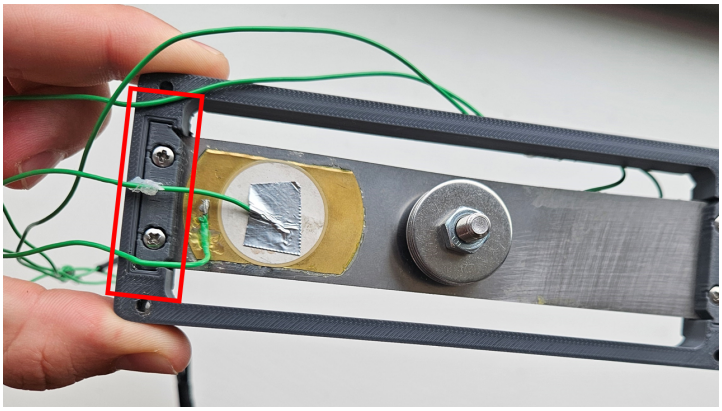


Figure E.2: Bistable harvester, where the clamping part is indicated by the red rectangle. The flexure is clamped between two 3D printed surfaces and fixed by friction.

This likely happened after snap-through, where the abrupt deceleration causes a peak force (in tension) on the clamped part. When this happens, the characteristics of the harvester change within the experiment, which is undesirable. To mitigate this issue, the harvester is first put on the shaker with a high acceleration so that it constantly snaps through. Over time, the flexure will shift inwards, and it will reach a fixed position if 1) the bolts will touch the holes in the flexure, creating a form-closed joint (Figure E.3), or 2) the friction between the clamps and the flexure is higher than the peak force after snap through. After the flexure has a fixed position, it does not slip anymore since the (static) compressive forces are relatively low compared to the dynamic forces that occur after snap through. One easy way to check if the flexure is force-enclosed or form enclosed, is to use a multimeter and check if there is a short circuit between the bolt and flexure.

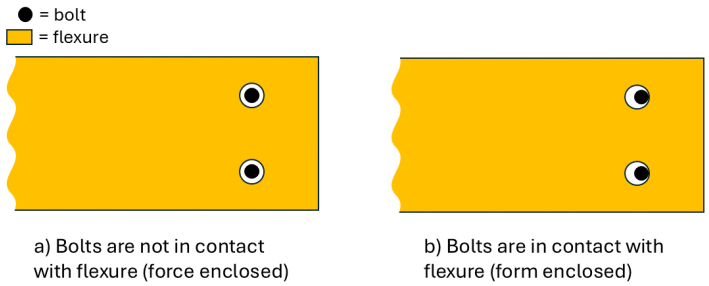


Figure E.3: Visualization of slipping of the flexure within the clamp. a) shows the flexure after assembly b) shows the flexure after a high tension force is put on it, and the flexure cannot slide anymore.

To eliminate the effect of errors due to creep and sliding, all measurements were taken directly after each other so that they could be performed over the span of one day.

E.4. Unequal acceleration for system identification & testing.

The power profile of the piezoelectric cantilever was modelled and tested for an acceleration of approximately 0.6 G, which can be considered a moderately low excitation level. The tests with the double sine, reached peak accelerations ranging from 1.62-2.95 G's. After reflection, this experiment could have yielded better results if both the single and multi-sine vibrations were performed at similar levels, this would probably have prevented a frequency shift and thus gave better correspondence between the modelled and experimental results.
Nevertheless, this does show that even linear systems exhibit nonlinear properties and this needs to be accounted for.